Master in Chemical Engineering

Influence of Atmospheric Plasma Spray Coating in Electrode Properties to Use in Alkaline Electrolysis

A Master's dissertation

of

Daniela de Aguiar e Azevedo

Developed within the course of Dissertation

held in

DLR / Institute of Engineering Thermodynamics

Deutsches Zentrum
DLR für Luft- und Raumfahrt

Supervisor at FEUP: Prof. Adélio Mendes

Supervisor at DLR: Regine Reiβner

U.PORTO
FEUP FACULDADE DE ENGENHARIA
UNIVERSIDADE DO PORTO

Department of Chemical Engineering

July 2017

Acknowledgments

First of all, I would like to thank to DLR, Institute of Engineering Thermodynamics, for giving me the opportunity of doing my master thesis with them and for the financial support. A big thank you to my supervisor at DLR, Regine Reiβner, for the help and guidance during my work in DLR, and a special thank you for the effort of reading my thesis in the last days. To all the people involved in my work and that somehow contributed to it; to Dr. Liu Taikai, that helped me understanding the SEM images, to Li Wang who helped me so much understanding Cyclic Voltammetry and UPD; and, of course, thank you to all the people who was involved in the XRD and EDX analysis and in the Atmospheric Plasma Spraying.

To Prof. Adélio Mendes, thank you for presenting this opportunity and for all the advices and help before coming to DLR. To Prof. Miguel Madeira for all the support before and during my stay in DLR and to all the professors in FEUP that contributed to my professional growth during my academic path.

To SASUP (Serviços de Acção Social da Universidade do Porto) I want to thank you for the important financial support to make this adventure possible. To the Cooperation Division in FEUP that helped me with all the bureaucracy and procedures to come abroad.

To my family and friends in Portugal that were always one click of the mouse away for me during my time here. I would like to thank specially to my mom, dad, brother, Elisabete, Rute and Ana Faria who helped me when I was “freaking out” and to my parents, especially for the financial support.

To all the people I met in Stuttgartr who made me feel less lonely and home sick, specially to Melanie and Diana, for discovering Europe and Germany with me. A big thank you for the lunch times, coffee breaks and for the company in the office to my colleagues in DLR ;) To my roommates, specially Martin, for the beer-evenings and the so important company you made. To Tuxa Martins for being the friendly piece of Portugal in these foreign lands and for giving me a ceiling in my last days in Stuttgart.

Abstract

Hydrogen has been increasingly used as an energy carrier over the past few years due to its several applications mainly associated with the use of renewable energy. Among all the processes for hydrogen production, water electrolysis produces the purest hydrogen. However, the usage of water electrolysis accounts to only 4% of today's hydrogen production, mainly due to economic factors. Alkaline electrolysis is, so far, the most mature, the most efficient and the simplest process among the different types of electrolysis. Nevertheless, improvements in the process are still needed, especially in decreasing the cost of the process.

Nickel is one of the cheapest metals having also high electroactivity for oxygen and hydrogen production reactions. Raney-nickel materials, which are porous Ni, are the most promising electrocatalysts providing a wide surface area for the reactions to take place. Ni substrates coated with Raney-nickel NiAlMo using Atmospheric Plasma Spraying (APS) are promising stable cathodes due to the reduction of 0.226 V in hydrogen evolution reaction and its stability for, at least, 40 days. Cathodes produced with different APS parameters proved that high speed plasma jet at 580 $m.s^{-1}$ creates the most stable and electrochemically active coating.

Ni substrates coated with Raney-nickel NiAl coating were used for anodes. An increase of surface area towards uncoated Ni was achieved with porous NiAl. Adding Co_3O_4 to the NiAl coating a decrease in 0.1 V for oxygen evolution and a stable sample that lasted for 35 days was achieved, mainly due to the presence of Co.

Underpotential deposition, as technique to calculate the surface area of a Ni electrode was studied. As expected, Ag was adsorbed in the Ni surface, which was identified by the several increases in current during the cyclic voltammogram cycles due to oxidations and reductions of adsorbed Ag.

Keywords: alkaline electrolysis, hydrogen evolution reaction, oxygen evolution reaction, NiAl alloy, Atmospheric Plasma Spray, potential reduction, Under Potential Deposition.

Sumário

O hidrogénio tem sido usado como vetor energético ao longo dos últimos anos devido às suas variadas aplicações, nomeadamente associadas ao uso de energias renováveis. De entre todos os processos para a produção de hidrogénio, a eletrólise da água produz o hidrogénio mais puro. Contudo, o uso de eletrólise representa apenas 4 % da atual produção de hidrogénio, principalmente devido a fatores económicos. A eletrólise alcalina da água é, até ao momento, o processo mais estudado, eficiente e simples entre os vários tipos de eletrólise. No entanto, melhoramentos são ainda necessários, especialmente no que toca aos custos associados que precisam de ser reduzidos.

Níquel é um dos metais mais baratos e possui elevada eletroatividade para as reações de produção de hidrogénio e oxigénio. Raney-níquel, i. e. níquel poroso, é um dos mais promissores eletrocatalisadores, tendo uma larga área superficial onde as reações podem decorrer, apesar da pouca estabilidade quando operando a longo prazo. Um substrato de Ni revestido com uma mistura de NiAlMo poroso (Raney-níquel) usando o método de revestimento Metalização por Plasma à Pressão Atmosférica (APS) foi estudado como cátodo. Os resultados obtidos mostraram ser promissores, tendo sido obtida uma redução no potencial de 0.226 V para a evolução do hidrogénio. A melhoria dever-se-á à presença de Mo e à utilização de APS como técnica de revestimento que aumentou de forma significativa a área superficial do elétrodo. A velocidade do jato de plasma introduz diferenças nos revestimentos. O elétrodo revestido usando um jato de plasma com maior velocidade mostrou ser o elétrodo mais estável, tendo o revestimento aguentado 32 dias, até o teste ser parado.

Substratos de Ni revestidos com NiAl Raney-nickel foram usados como ânodos. Um aumento na área superficial face à área de Ni não revestido foi possível com revestimento de NiAl poroso. Adicionando Co_3O_4 ao revestimento de NiAl poroso foi possível obter uma redução de 0.3 V para a reação de formação de oxigénio e um revestimento que durou, pelo menos 35 dias.

A deposição de metais a potencias menores que o previsto pela lei de Nernst foi estudada como uma técnica para calcular a área superficial de um elétrodo de Ni. Foi utilizada Ag como o metal a ser depositado e a deposição de uma monocamada de Ag foi identificada, tendo os primeiros testes sido bem-sucedidos.

Declaration

I hereby declare, on my word of honor, that this work is original and that all non-original contributions were properly referenced with source identification.

Daniela Aguiar Azevedo

31/07/2017

Table of contents

Notation and glossary

A	Frequency factor	s^{-1}
a_x	Activity of component x	
Δ	Difference operator	
E	Electrode reduction potential	V
E_a	Activation energy	J
F	Faraday constant	96485.34 $C \cdot mol^{-1}$
G	Gibbs free energy	J
i	Current	A
i_0	Exchange current density	$A \cdot m^{-2}$
j	Current density	$A \cdot m^{-2}$
k	Reaction rate	s^{-1}
n	Number of electron transferred	
NLpM	Normal Liter per Minute	
η	Efficiency	%
R	Electrical resistance or gas constant	Ω or 8.314 $J \cdot K^{-1} \cdot mol^{-1}$
T	Temperature	K
wt	Weight in percentage	%

Subscript/Superscript

0	Standard (25 ^{o}C, 1 atm)
ads	adsorption
i	index or counter

List of Acronyms

APS	Atmospheric Plasma Spraying
bcc	Body centred cubic structure

CE	Counter Electrode
DLR	Deutsches Zentrum für Luft- und Raumfahrt e.V.
EIS	Electrochemical Impedance Spectroscopy
fcc	Face centred cubic structure
HER	Hydrogen Evolution Reaction
OCV	Open Cell Voltage
OER	Oxygen Evolution Reaction
ORR	Oxygen Reduction Reaction
PEM	Proton Exchange Membrane
RE	Reference Electrode
RESelyser	“Hydrogen from Renewable Energy Power Sources”
RHE	Reversible Hydrogen Electrode
SHE	Standard Hydrogen Electrode
SEM	Scanning Electron Microscopy
SOEC	Solid Oxide Electrolysis Cell
UPD	Under Potential Deposition
VPS	Vacuum Plasma Spraying
WE	Working Electrode
XRD	X-Ray Diffraction

1. Introduction

1.1. Framing and presentation of the work

The use of hydrogen as an energy carrier is becoming increasingly important over the years. Hydrogen can be used as a fuel in fuel cells and internal combustion engines, has high gravimetric energy density i.e. up to three times larger than liquid hydrocarbon fuels and has small environmental issues [1]. Additionally, it can be used as a reducing agent in several catalytic processes in chemical industry, as for instance in ammonia synthesis. It is relatively abundant in nature and can be produced using renewable or non-renewable sources. Hydrogen production via water electrolysis amounts to only 4% of today's hydrogen production, mainly due to economic factors [2]. The use of this process and hydrogen usage as fuel requires appropriate infrastructures and huge investments [1]. However clear advantages of hydrogen production by means of water electrolysis as the high efficiency of the process and the high purity of the produced hydrogen make the process worth to be studied. In order to promote the development of water electrolysis, intensive studies have been done as a number of exciting new innovations in the last few years.

There are different categories of water electrolysers depending on the electrolyte used and operation temperature. They are alkaline electrolysis, proton exchange membrane (PEM) electrolysis and solid oxide electrolysis (SOE). Alkaline water electrolysis is seen as the most promising method for high purity and highly efficient hydrogen production since it offers the advantage of simplicity of process and uses less expensive materials [3]. However, some challenges must yet be solved, mainly because of the low purity of oxygen gas, low current densities and high overpotentials. At the moment, Ni is the most common material used in the electrodes, however it loses activity quite fast. As an answer to this problem, coated Ni is being used instead of pure Ni. Several techniques can be used to fabricate coated electrodes, as cathodic codeposition, gas atomization, composite coating, or thermal spray [4]. However, the conventional preparation methods for electrode coatings exhibit considerable disadvantages. For example, thermal processes may origin undesired decomposition or phase transformations and in the end, can only achieve thin layers that presents low mechanical stability. Galvanic deposition is restricted to just a few metals and alloys and is also associated to some environmental issues [5]. Although VPS (Vacuum Plasma Spraying) has created high performance electrodes for alkaline water electrolysis, is an expensive and complex technique. In this work, APS (Atmospheric Plasma Spraying), a similar method to VPS at atmospheric pressure, was used to produce the coating of the electrodes.

1.2. Presentation of the company

The presented work was accomplished in the German Aerospace Center (DLR), in the Institute of Technical Thermodynamics in Stuttgart. DLR is an aeronautics and space research center whose extensive research and development in aeronautics, space, energy transport and security is integrated into national and international cooperative projects. The headquarters of DLR are located in Köln although DLR has approximately 20 more facilities locations in Germany and offices in Brussels, Paris, Tokyo and Washington D.C.. The Institute of Engineering Thermodynamics in Stuttgart does research in the field of efficiency energy storage systems that conserve natural resources, and next generation energy conversion technologies [6].

1.3. Contributes of the work

This thesis is based on previous work in a European project called “RESelyser – Hydrogen from RES”, whose purpose is to develop “high pressure, highly efficient, low cost alkaline electrolyzers that can be integrated with renewable energy power sources using an advanced separator concept, highly efficient electrodes and a new cell concept” [7]. It contributes to the project “Leuchtturmprojekt Power-to-Gas - Angewandte Forschung und Entwicklung für eine ökonomische Erzeugung des ökostrombasierten Kraftstoffs eH2” supported by the state of Baden-Wuerttemberg of which one of the tasks is to integrate advanced components like new electrodes in a 300 kW alkaline electrolyser.

1.1. Organization of the thesis

The thesis is organized in 5 chapters:

- 1st chapter is the introduction of the work and company;
- 2nd chapter is the state of the art related to this work;
- 3rd chapter explains the materials and methods applied in this work;
- 4th chapter discusses the results obtained;
- 5th chapter presents the conclusion of the work and some suggestions for a future work.

2. Context and State of the art

2.1. Alkaline water electrolysis

Electrolysis is a technique that uses direct current to drive non-spontaneous reactions. An electrolysis unit consists of two electrodes, the anode and the cathode, an electrolyte and a power supply as represented in Figure 1. Water electrolysis, in particular, uses an input of current and water to produce hydrogen and oxygen gases. If it is alkaline water electrolysis then an alkaline electrolyte is used.

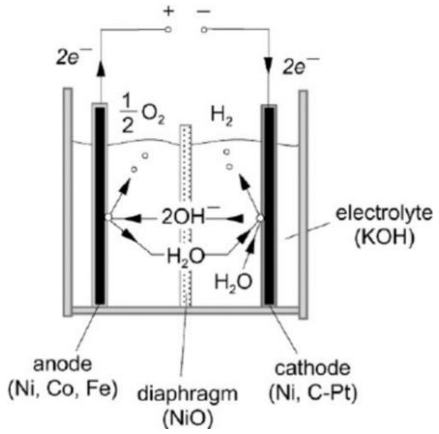

Figure 1 – Illustration of an alkaline water electrolysis unit. [8]

The power supply applies a current between the electrodes, decomposing the water into hydrogen and oxygen. In this process, the water molecules are reduced in the cathode, hydrogen evolution reaction (HER), equation (1), and the hydroxide ions are oxidized in the anode, oxygen evolution reaction (OER), equation (2), according to the followings equations.

Cathode: $2H_2O + 2e^- \rightarrow H_2 + 2OH^-$ (1)

Anode: $2OH^- \rightarrow \frac{1}{2}O_2 + H_2O + 2e^-$ (2)

Overall reaction: $H_2O \rightarrow \frac{1}{2}O_2 + H_2$ (3)

The electrodes are conductive materials, usually metals, which allow the electrons to flow and where the reaction happens. As it is represented in Figure 1, the electrons flow from the anode to the cathode through the cables and the power supply. The electrolyte is a conductive solution that allows the ions to move, but not the electrons, thus maintaining the electrical charge in balance and enabling the reaction to occur. Several parameters influence the extent of the electrolysis as the electrodes material, the electrolyte composition, the operating conditions, as temperature and pressure, the cell´s setup among others.

In this way, voltage can be seen as a measure of the cell efficiency. The x-axis is the current density, i. e. the current normalized by area of the electrode, to make the results comparable as the current and voltage are proportional to the electrode area. An ideal cell would supply any amount of current (as long as it is supplied with enough fuel), while maintaining a constant voltage. However, there are several losses in the process causing a real cell to have a performance as seen in the previous **Error! Reference source not found.** [9].

2.1.1. Resistances

They result of the existence of some barriers that must be overcome so that the reaction can proceed. These are the electrical resistance of the circuit, the activation energies of the electrochemical reactions occurring on the surfaces of the electrodes, the availability of electrode surface due to partial coverage by gas bubbles formed and resistances to the ionic transfer within the electrolyte solution. Figure 2 summarizes the resistances involved:

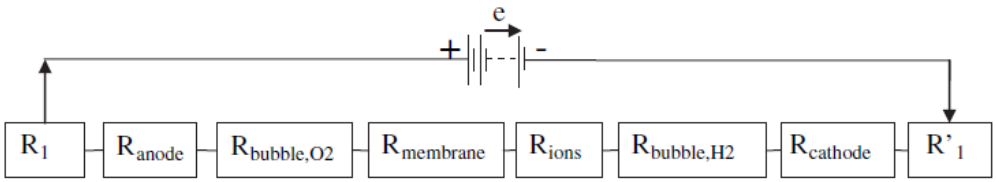

Figure 2 – Schematic representation of the resistances in a water alkaline electrolysis unit. [10]

As seen before, the reaction that takes place in an electrolysis cell is not spontaneous. Therefore, some energy must be supplied to the system in order to make it happen. The equilibrium cell voltage, or electromotive force, can be defined as the equilibrium potential difference between the anode and the cathode when working as an open cell. For water, at 25 ^{o}C and 1 bar, this value is 1.23 V. For a real cell, however, because there are a series of resistances, an input of additional energy must be given. This is measured as overpotential, the extra voltage needed to kick start the reaction exceeding the theoretical minimum voltage. This start energy must overcome the activation energy, but even for the reaction to proceed is necessary more than the theoretical voltage since there are still losses in the system.

It is widely accepted that HER in alkaline solution goes through these steps:

$$H_2O + M + e^- \rightleftharpoons MH_{ad} + OH^- \quad (4)$$

$$MH_{ad} + H_2O + e^- \rightleftharpoons M + H_2 + OH^- \quad (5)$$

$$MH_{ad} + MH_{ad} \rightleftharpoons 2M + H_2 \quad (6)$$

The adsorption of H, equation 4 also called Volmer equation, is believed to be the rate determining step. If more surface area is available to the adsorption of H to take place, then the following reactions can be faster [10].

OER mechanism is more complex, however it is most generally accepted to have the following steps:

$$OH^-_{ads} \rightleftharpoons OH_{ads} + e^- \quad (7)$$

$$OH^- + OH^-_{ads} \rightleftharpoons O_{ads} + H_2O + e^- \quad (8)$$

$$O_{ads} + O_{ads} \rightleftharpoons O_2 \quad (9)$$

The adsorption reactions are, as in HER, important steps for oxygen production. Therefore, an increase in the surface area is advantageous also in the anode side. However, may not be enough due to the low kinetics of this reactions and catalysts must be added, as it will be shown in the next chapters.

2.1.2. Thermodynamics

The equilibrium cell voltage can be related with the Gibbs free energy using the following equation:

$$\Delta G^o = nFE^o \quad (10)$$

where ΔG^o is the standard-state Gibbs energy, n is the number of moles of electrons transferred, F is the Faraday number and E^o is the standard-state equilibrium cell voltage.

The Nernst equation gives the equilibrium cell voltage at a certain temperature and pressure and electrolyte concentration and is as following:

$$E = E^o - \frac{RT}{nF}\ln\frac{a_{H_2O}}{a_{H_2}a_{O_2}^{1/2}} \quad (11)$$

Where E is the equilibrium cell voltage in the desired conditions, E^o is the standard-state equilibrium cell voltage, R is the gas constant, T the temperature, n is the number of electrons involved and a are the activities of water, hydrogen, and oxygen. With these equations, it is possible to calculate the theoretical value for the equilibrium cell voltage in order to calculate the cell efficiency. One common way of expressing cell efficiency is to relate the energy input with the energy output as in the following equation [10]:

$$\eta = \frac{E_{cathode} - E_{anoode}}{E_{cell}} \quad (12)$$

Several innovations have been made towards increasing the efficiency, for instance reducing the overpotential, which can be done by amending the electrodes composition or/and structure.

2.1.3. Kinetics

In addition to thermodynamics also the kinetics of the electrode reactions affects the performance of electrochemical cells. The reaction kinetics can be expressed by means of current density and the rate constant of a reaction is described mathematically by Arrhenius equation as in Equation 10 [10].

$$k = A \cdot e^{\frac{E_A}{R.T}} \quad (13)$$

Where *k* is the rate constant, *A* is the frequency factor and E_A is the activation energy. A relationship between the rate constant and the geometry of the electrode, temperature and activation energy of the reaction is shown. The kinetics mostly depends on the electrode surfaces and on the behaviour of the electrolytic solution adjacent to the electrodes, where the double layer effect happens. The double layer effect is created by accumulation of ions that adds resistance to the system [10]. The double effect is explained in Appendix A.

The dependence on the temperature can be explained considering the mechanisms present in the electrolysis. The increase of temperature promotes ions movement, raises the reaction speed, and increases the cell efficiency by providing extra energy to the reaction. An increase in temperature reduces also the cell overpotential, as seen in Figure 30, Appendix A. Nevertheless, other mechanisms take place during the process that are not temperature friendly, for instance, a temperature too close to the water boiling temperature would increase the water loss by evaporation. Finally, high operation temperatures carry more problems to the structural integrity of the materials. Accordingly, some authors concluded that alkaline water electrolysis must be done in a range of 70-80 ^{o}C [10].

The electrolyte concentration influences the cell performance as well. A higher concentrated electrolyte has a higher conductivity however, the conductivity is also temperature dependent. Previous studies found that for a cell operating between 70-80 ^{o}C the conductivity of a 30 % KOH solution is maximum [7].

2.2. Electrodes

2.2.1. Cathodes

Nickel is the most common electrocatalyst for hydrogen evolution reaction (HER) owning to its low cost, good catalytic activity, and high chemical stability in the alkaline environment. Nevertheless, it faces problems of deactivation, since the HER activity of nickel cathodes is significantly greater on fresh electrodes than after long-term operation [1] [11]. This happens because of transformations occurring on the surface of the electrode. Using a variety of electrochemical and physicostructural

characterization techniques it was found that fresh electrodes are covered with α-nickel(II)hydroxide, α-$Ni(OH)_2$, and some nickel oxide, NiO_x, which are reduced to metallic Ni during HER [12] [1].

Some studies show that the presence of α-$Ni(OH)_2$ improves HER activity when compared to Ni without any $Ni(OH)_2$ [1] [13]. In alkaline media, α-$Ni(OH)_2$ gradually transforms into β-$Ni(OH)_2$ which has a crystalline structure and is more stable than α-phase [12] [14]. The effects of β-$Ni(OH)_2$ are not yet fully understood however some studies suggest that it can reduce the overpotential of the electrode towards HER [12]. After repeated oxidation-reduction cycles the formation of α-$Ni(OH)_2$, β-$Ni(OH)_2$ and NiO_x and its reduction to metallic Ni develop strains on the surface of the electrode decreasing HER activity due to damages on the electrode [1]. This decrease is even more pronounced after several hours of electrolysis, and especially when exposed to high alkaline solution and high current densities, because of an extensive formation of α-NiH_x and β-NiH_x. The hydrates are formed due to large extent of hydrogen incorporation and act as a barrier to H diffusion. The addition of H into the electrode alters the electronic structure in the interface and adversely affects the HER activity [1] [14]. Therefore, some changes in the electrodes must be made to improve its performance.

2.2.1.1. Raney-nickel electrode

Some electrocatalytic studies indicate Raney-nickel as the most active electrocatalyst for hydrogen evolution [12]. Raney-materials are alloys of which one phase is leached out in an activation process becoming a porous material with a very high surface area [7]. In a PhD thesis by S. Knies, an area of of 64 $m^2 \cdot g^{-1}$ after leaching was achieved. Usually they are made with nickel and aluminium or nickel and zinc being Al and Zn the leached components. As the performance of the electrode is proportional to its electrochemically active surface area, since the reactions involved are inherently surface processes, this material has also a better performance [15]. Beyond the surface area, NiAl intermetallic compounds are responsible for other attractive properties as the corrosion resistance and temperature yield strength [16]. The cooling down process after sintering creates different phases, with different chemical formula and structure, depending on the Ni/Al ratio. On a phase diagram, it appears as an intermediate phase that exists over a very narrow range of compositions. This phase is formed because of the difference in electronegativity between the Al and Ni that allow them to rearrange during the cooling down process when a diffusion process takes place [17]. The final ordered structure exhibits superior elevated-temperature properties because of the long-range-ordered superlattice, which reduces dislocation mobility and diffusion processes at elevated temperatures [18]. The phase diagram for NiAl system is represented in Figure 3. These dendritic structures have been found to increase the ductility of compounds and cannot be leached in KOH solution [19].

Daniel Chade et al. reported that, at a temperature of 70 °C, the potential for HER was -0.95 V vs Hg/HgO for a 50/50 NiAl sample with a thickness of 30 µm in a 30 % KOH bath.

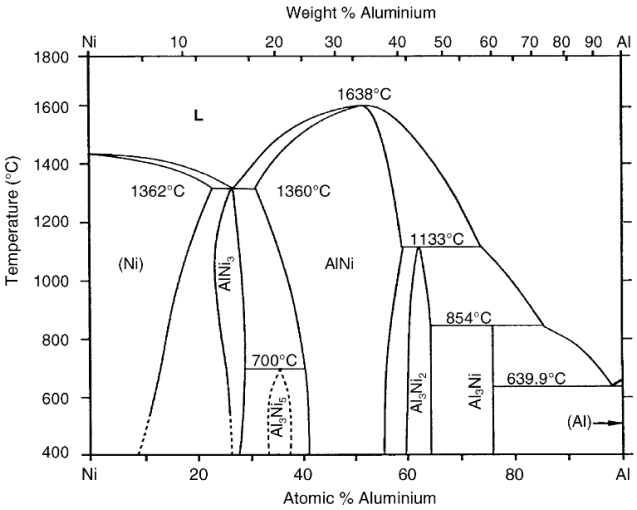

Figure 3 – Ni-Al Pourbaix diagram [20].

2.2.1.2. Mo-containing Raney-nickel electrode

In order to improve the stability of the electrode during intermittent operation, some authors proposed molybdenum-containing Raney-nickel alloys as an interesting material for cathodes. The addition of molybdenum increases the corrosion resistance and has low overpotential for HER [7] [21]. Although the reason to this behaviour is not yet fully understood, some hypotheses have been proposed to clarify it. It is believed that a very strong bond is created when Ni, Al and Mo are alloyed based on the theory that Mo has half-filled d-orbit and Ni has conjugated d electrons. The strengthened bond generates a better electrode structure that benefits electron transport and consequently improve the HER electrocatalytic activity and stability of the electrode [22]. According to Liang Wu et al. the overpotential of a porous molybdenum-containing Raney-nickel (NiAlMo) electrode sintered in a vacuum furnace at high temperature decreased with time during the first 48 h. Then the overpotential became constant.

In the present work, metallic nickel was coated with NiAlMo using a recent technique called Atmospheric Plasma Spray (APS) and was tested afterwards.

2.2.2. Anodes

Particular improvements are required for the anode side where the oxygen evolution reaction (OER) takes place. The high overpotential occurring at the anode, as a result of the sluggish kinetics of OER, is the major source of energy loss during water electrolysis. At the moment, noble metals are the

most active materials for OER during water electrolysis. However, either they suffer from deactivation in alkaline environment or they are too expensive or even rare on earth. Therefore, low cost transition metal oxides are typically used in alkaline water electrolysis due to their abundancy, low cost and relatively high activity and stability [1].

Nickel-based oxides are the most promising materials for OER in alkaline media since they show good activity and have high corrosion resistance in this environment. The good performance of metallic Ni in comparison with other transition metals lies on the transformations that take place on its surface. As explained before for cathodes, when Ni is immersed in an alkaline solution, a layer of $Ni(OH)_2$ instantaneously grows on top of the air-formed NiO layer. Therefore, a NiO layer is in contact with the electrode and a $Ni(OH)_2$ layer is exposed to the alkaline solution, each layer having a different role in the OER [23]. In one hand, $Ni(OH)_2$ is oxidized into NiOOH and reduced back every potential cycle, as in Equation 14.

$$Ni(OH)_2 + OH^- \rightleftharpoons NiOOH + H_2O + e^- \quad (14)$$

Two phases of both $Ni(OH)_2$ and NiOOH can exist, the α-phase and the β-phase. After consecutive potential cycling in a strong base, α-phase gradually transforms into β-phase, which is more crystalline and therefore more stable than α-phase. It was suggested that β-$Ni(OH)_2$ phase is also more active for OER since its oxidation to β-NiOOH represents the optimal condition for the OER to occur due to its structure. The latter can also increase the surface roughness thus promoting the detachment of bubbles and leading to a higher OER activity. In the other hand, some studies show that after deterioration, NiO grows and creates an oxide film protecting the inner layers against redox reactions. Since the repeated oxidation-reduction cycles create strains in the electrode, as seen for cathodes, the oxide film gives stability to the electrode [1] [23].

In order to improve the catalytic performance of the nickel electrode numerous studies have been made combining Ni with other elements and using several preparation methods.

2.2.2.1. NiAl electrode

Doping Ni with Al creates an alloy that exhibits excellent isothermal and cyclical oxidation resistance. The pore structure remains stable due to the formation of a very thin and discontinuous layer of alumina oxide that is formed at very high temperatures. A porous NiAl sample was prepared by H. X. Dong et al. and tested in cyclic oxidation in air at high temperatures. They showed that after 110 h at 400 ^oC no oxidation took place on the surface, but with the increase time and heating temperatures, the increase of oxygen content over the surface can be found [16].

2.2.2.2. NiO electrode

A NiO electrode obtained by oxidizing a Ni plate at high temperatures shows more stability than bare Ni because of the protective function of the oxide layer. However, is also less active since $Ni(OH)_2$ is not present [24]. At 25 ^{o}C in 7.0 mol·L^{-1} KOH H. Ichikawa et al. studied the performance of NiO electrodes produced by metallic Ni oxidation at 1000 ^{o}C. It was shown that the potential of NiO only slightly increases with potential cycling after 25000 cycles.

2.2.2.3. Co_3O_4 modified Ni electrode

The addition of Co_3O_4 to pure Ni electrodes was studied in DLR before. It was observed that it leads to a significant improvement for OER current density and also leads to an increase of electrode stability. However, an optimum ratio between Co_3O_4 and Ni must be used because of Co_3O_4 high electronic resistance [11]. A mechanism for OER involving the electrochemical adsorption of OH^- preferentially in Co(IV) active sites was suggested. Since the Co(III) existing in Co_3O_4 can be oxidized to Co(IV), its presence enhances OER activity [25]. The stability increases as well due to the preferential use of Co as active site for HO^- adsorption instead of Ni. Consequently, Ni does not go through the repeated oxidation-reduction cycles that create the strains in the electrode structure leading to its destruction. Additionally, because the presence of Co_3O_4 creates a different structure in the electrode, the roughness factor of the surface increases and thus the surface area [26]. At DLR, Dennis Wittmeir et al. prepared several electrodes using different amount of Co_3O_4, Ni and a PTFE binder. Co_3O_4 20 w t% turned out to be the optimum with the OER occurring around 1.5 V vs RHE and showing only a slight increase in the potential for 1200 cycles. G. Schiller et al., investigated Raney-nickel/ Co_3O_4 matrix anode coatings produced by VPS technique that showed high electrochemical performances in alkaline water electrolysis. Its operation in electrolysers exhibited a stable mechanical and electrochemical behaviour during long-term tests using constant and intermittent power supply for more than 10 000 h [5].

2.2.2.4. Ag/Co_3O_4 electrode

DLR also recently reported a highly active and stable catalyst combination of Ag/Co_3O_4 which reaches high current densities at low overpotential for OER. Ag has the highest electric conductivity of all metals, which compensates the low electric conductivity of Co_3O_4. However, this combination at high potentials was shown to be unstable under ambient conditions and the electrode starts to decompose within hours after removal from the half-cell. The high instability of this electrode was attributed to a possible reaction of silver oxides with KOH [27].

2.2.2.5. P-containing Raney-nickel electrode (NiAl) treated at high temperature

Concerning only the corrosion resistance of the Ni electrode, a new coating technique called electroless Ni-P deposition was developed. Among the excellent properties of P-containing coatings are the uniform thickness, high hardness and high wear resistance of the electrode due to increase in surface roughness and intrinsic activity [28].

In this work, four different coating compositions were tested, all of them deposited on a metallic Ni spreadsheet using APS. The coatings tested were Raney-nickel (NiAl), CO_3O_4-containing Raney-nickel (NiAl) with two different particles size of CO_3O_4, Ag/CO_3O_4-containing Raney-nickel (NiAl), Raney-nickel (NiAl) treated at high temperature and P-containing Raney-nickel (NiAl) treated at high temperatures.

2.3. Atmospheric Plasma Spraying

Atmospheric Plasma Spraying (APS) is a thermal spray coating technique in which a powder is melted, accelerated, and deposited on a substrate creating a layer. In this process, a direct current is applied in the positive pole (cathode), which arcs to the negative pole (anode). This current ionizes the gases, which are introduced along the cathode, into the plasma state. Then, the powdered feedstock material is injected into the plasma jet where is melted and accelerated and then is propelled trough the nozzle onto the electrode substrate surface. The basic work principle is the same as for Vacuum Plasma Spray (VPS) with the advantages that it is cheaper and less complex since no vacuum is needed [29].

Figure 4 shows the cross section of a typical plasma gun.

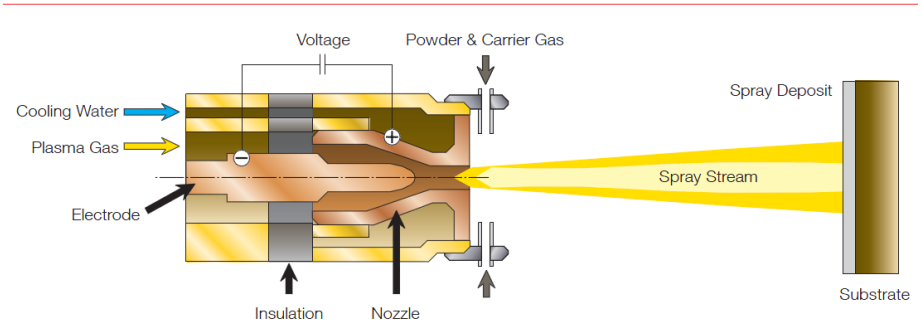

Figure 4 – Illustration of a cross section of a typical thermal plasma gun. [29]

The primary gas is usually Ar however additives as nitrogen, hydrogen, helium, and oxygen can be used to have the desired results. For example, adding hydrogen, nitrogen or helium increases the heat transfer to the powder, raise the plasma jet enthalpy, and extend the hot range of the jet resulting in improved melting conditions. Therefore, the stability and deposition efficiency are

improved. Oxygen can also be added to the powder carrier gas, creating different levels of oxidation through reactions with the particles [5].

Other parameters can be amended to achieve the desired results as the plasma speed and its temperature and the nozzle geometry and its distance to the substrate. They affect the surface area, the layer density, adhesion of the coting to the surface, its cohesion and porosity. In this work, different parameters were studied to understand how they affect the electrode electrochemical and long term behaviour of the electrode.

2.4. Characterization techniques

Some of the most common techniques to analyse the structure of the samples are SEM (Scanning Electron Microscopy), EDX (Energy-Disperse X-Ray Spectroscopy) and XRD (X-Ray Diffraction).

The electrochemical behaviour is commonly tested with Cyclic Voltammograms (CV) and Electrochemical Impedance Spectroscopy (EIS) although in the present work only CV was used.

Appendix B shows a brief explanation about the basic principles of these techniques.

Under-potential deposition (UPD)

The under-potential deposition (UPD) of metals refers to the deposition of metals on a foreign metal substrate at potentials more positive than the predicted by the Nernst equation for its bulk deposition. The deposition at more positive potential can be interpreted as a result of a strong interaction between the electrodepositing metal and the substrate. Some studies suggest that the binding energy for the adsorbed atoms on the substrate exceeds the binding energy of the atoms in the respective bulk crystal. It is deduced that the electrodeposition typically occurs only up to one or two monolayers [30]. Copper UPD on iridium and silver UPD on platinum were previously studied due to its important implications in industry as coating technique. Since usually only a monolayer of the metal is deposited under the substrate, UPD can also be used to calculated surface areas. In order to understand if Ag can also be used for UPD on Ni electrodes in alkaline electrolysis the behaviour of Ag in alkaline environment and under different potentials must be understood.

3. Materials and Methods

3.1. Atmospheric Plasma Spaying (APS)

To produce the coatings Triplex-APS-Pulver-Spitzprotokoll DC-1 was used.

3.1.1. APS parameters

The coatings of the cathodes were produced using the parameters indicated in Table 1. A 2 bar air jet was used to cool down the substrate, preventing its melting and the spraying distance was 60 mm.

Table 1– APS parameters for coating process for cathodes: temperature, velocity, time exposure, amount of gases and power net.

Sample	T (°C)	v (m/s)*	t (µs)**	Flame lenght (mm)	Ar (NLpM)	H_2 (NLpM)	Power net (kW)
T17.001	2510	239	251	30	40	2	18.2
T17.002	2395	290	207	35	60	3	25.2
T17.003	2370	350	171	40	80	4	31.1
T17.004	2445	416	144	45	100	5	35.1
T17.005	3125	580	103	50	120	4	42.0

* The velocity was measured at 170 mm from the spray jet.

** The time was calculated with the velocity measured for a distance of 60 mm.

The coatings of the anodes were produced using 80 NLpM of Ar, 4 NLpM of H_2 and a power net of 30 kW.

3.2. Test bench

The electrochemical tests were carried out in half-cell arrangement with a three-electrode setup, consisting of a working electrode (WE), a counter electrode (CE) and a reference electrode (RE). The APS coated samples with a geometric area of 4 cm2 were the working electrode. As counter electrode, an expanded metal sheet of metallic Ni was used. Although the same CE was used for different tests with different WE, it was not used as both cathode and anode. All potentials are referred to the reversible hydrogen electrode, RHE (HydroFlex, Gaskatel). A solution of 30 % KOH was used as electrolyte and it was prepared using distilled water and KOH pellets (purity ≥ 85 %) The

temperature of the bath was kept at 70 ^{o}C. To high values of current, until 1 A·cm^{-2}, another power supply was used as a source of energy, and the interface ProfiSignal Version 4.2.0.7 recorded the voltage applied and the response of the system. To smaller values of current and to obtain more precise readings the interface Thales 23.04 was used for both delivering electrical power and measure the response of the system. Figure 5 shows an illustration of the electrode holder and the half-cell set-up used.

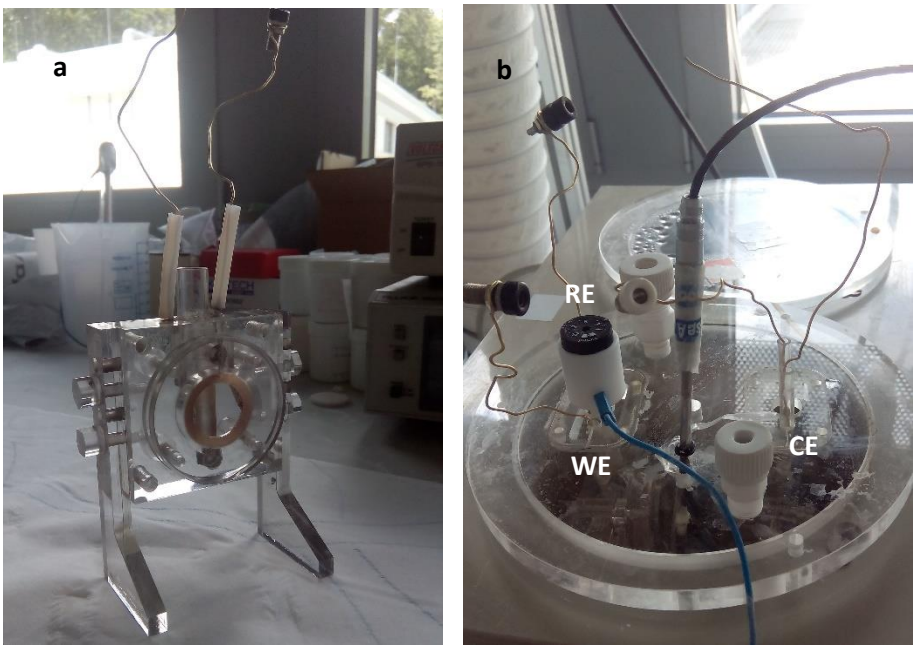

Figure 5 – Illustration of the electrode holder used (a) and of the set-up (b).

3.3. Electrodes

The substrate used for cathodes was stainless steel punched hole sheets of galvanically plated nickel, 0.5 mm thick and with a geometrical area of 4 cm^2. For the anodes, the substrate used was nickel expanded metal sheet also with a geometrical area of 4 cm^2. Before the coating, substrates went through a sand-blasting process to remove the oxide layer and roughen the surface. All the substrates were coated in one side with APS using the conditions specified in chapter 3.1.1. Ni substrates are illustrated in Figure 6.

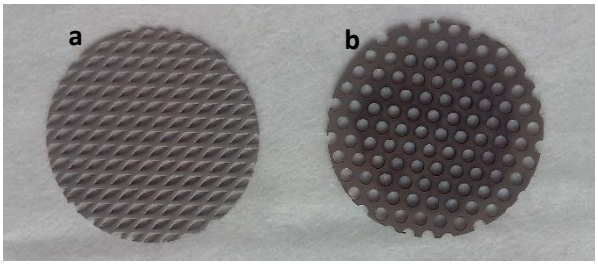

Figure 6 – Illustration of the Ni substrate used for anodes (a) and for cathodes (b).

The cathodes were coated with an active layer of NiAlMo (39/44/17 wt %).

The coatings used for anodes had different compositions for each sample, which are described in Table 2.

Table 2 –Composition of the coating of the anodes: composition, supplier, and pore size.

Sample	Composition and particle size
T17.025.5 (*) (**)	NiAl (56/44 wt %), 18 µm
T17.025.6	NiAl (56/44 wt %), 18 µm
T17.027.3	60 % NiAl (56/44 wt %), 18 µm 10 % Co_3O_4, 6.5 µm 30 % Co_3O_4, 18 µm
T17.028.3	30 % NiAl (56/44 wt %), 18 µm 10 % Co_3O_4, 6.5 µm 30 % Ag 30 % Co_3O_4, 18 µm

*Samples T17.025.4 and T17.025.5 went through a heating treatment after leaching. The treatment took place in a tubular reactor inside of a furnace, at atmospheric pressure and within a free-oxygen environment. In this case an Ar atmosphere was kept inside the reactor. During the process, a heating rate of 3 ^{o}C/min was used. The temperature rose until 300 ^{o}C where it was held for 2 h. Afterwards the sample cooled down inside the reactor to the room temperature and then it was stored in distilled water.

**Sample T17.025.5 was coated with sodium hypophosphite monohydrated ($H_2NaO_2P{\cdot}H_2O$). A mass of 3.52 g of sodium hypophosphite was mixed with distilled water in order to create a paste. The amount was calculated considering the use efficiency of hypophosphite, at the best conditions, i.e., that to deposit 1 g of Ni, 5 g of sodium hypophosphite are required [28]. The paste was spread on the activated area of the coated electrode which was immediately introduced inside the reactor to undergo the heat treatment. The reaction occurring in the surface is the following:

$$H_2PO_2^- + H_2O \rightleftharpoons H_2PO_3^- + 2H^+ + 2e^- \quad (15)$$

3.4. Electrochemical measurements

Electrochemical measurements were performed using the interface Thales 23.04. Different test benches were used, each with different impedance. Therefore, IR corrections were made to compare the performance of the samples. The correction was made using the following equation:

$$V_{iR\ corrected} = V_{measured} - i * R \quad (16)$$

3.4.1. Cyclic voltammetry

For the study of the electrochemical behaviour of the electrodes the parameters found adequate, as potential limits, slew rate and the number of cycles, for cathodes and anodes are shown in Table 3. To study HER in cathodes, the lower limit must be negative enough to see the hydrogen evolution. The upper limit of 1.5 V was chosen to avoid further reactions of taking place in the surface, preventing the cathode destruction. In case of the anodes, the upper limit must include the start of OER and the lower limit was chosen to prevent further reactions of taking place on the surface avoiding any more stress for it. Three cycles were made at each measure to give precision to the measurements. Finally, the slew rate value of 5 mV·s^{-1} was the one that allowed having a good quality of measurement and peaks big enough to be seen.

Table 3 – Potential limits, slew rate and number of cycles for cyclic voltammetry measurement for cathodes and anodes.

Cathodes

E_{start}	E_{lower}	E_{upper}	E_{end}
- 0.3 V	- 0.3 V	1.5 V	- 0.3 V
Slew rate		**Number of cycles**	
5 mV·s^{-1}		3	

Anodes

E_{start}	E_{lower}	E_{upper}	E_{end}
1.2 V	1.2 V	1.7 V	1.2 V
Slew rate		**Number of cycles**	
5 mV·s^{-1}		3	

3.4.2. Potentiostatic measurement

For the potentiostatic measurements, a frequency of 3 kHz was used. The amplitude for cathodes was 5 mV and for anodes was 10 mV. During all the potentiodynamic scans the ohmic resistance was registered to calculate the IR compensation. Both cathodes and anodes were tested in a linear potentiostatic measurement starting in OCV until the current reached 0.5 A·cm^{-2}. In order to reach higher values of current and analyse the electrode performance, another test was carried out using an external power supply and the interface ProfiSignal Version 4.2.0.7 for recording the current and voltage of the system. The linear potentiostatic measurement started at OCV and the current was increased until it reached 1 A·cm^{-2}. In all the scans, the current was held for around 10 s to 15 s for every measurement.

3.5. Experimental

3.5.1. Electrode tests

The APS prepared samples were first chemically activated. An aqueous solution of a 30% KOH (purity ≥ 85%) containing 10 % K-Na-Tartrate-Tetrahydrate (purity ≥ 99 %) in order to avoid aluminium hydroxide precipitation in the micropores of the Raney-nickel structure was used. The reaction that takes place during the leaching process can be written as:

$$\mathrm{Al\ (s) + OH^- \ (aq) + 3H_2O\ (l) \rightleftharpoons Al(OH)_4^- \ (aq) + \frac{3}{2}\ H_2\ (g)} \quad (17)$$

The formation of the complex bonding the aluminium ions is written in Equation 18

$$\mathrm{Al(OH)_4^- \ (aq) \rightarrow Al(OH)_3\ (s) + HO^- \ (aq)} \quad (18)$$

This process was carried out at 80 ^{o}C for 24 h. According to some studies, NiAl phase is stable below 90 ^{o}C. However, at this temperature NiAl phase is getting attacked resulting is some loss of material from the electrode and consequently in a too porous layer with lower stability [7]. Because a balance between high activity and stability must be achieved, the operation temperature was 80 ^{o}C.

Once activated, the electrodes were stored in distilled water since they are very sensitive to air and a reaction with it would make them loose much of their performance [7]. The activated electrode was then fixed in a half-cell support as in Figure 5. Before proceeding with any measurement, the electrode was operating at 0.5 A·cm^{-2} for around 15 min to reduce surface oxides present in the surface and to cathodically clean it. The potential was scanned linearly until 0.5 A·cm^{-2} was reached and then the cyclic voltammetry was performed. The potential limits and other parameters used for these measurements were the ones described in chapter 3.4.1. The operation mode for cathodes was different from the anodes in order to test both in the worst environment. The cathodes were tested in the first day and after 24 h in continuous operation at 0.5 A·cm^{-2}. Afterwards, the electrode was stored in a 30 % KOH solution at room temperature and OCV. The following tests were made after 1 week, 2 weeks and 3 weeks. The anodes were also tested in the first day and after 24 h in continuous operation at 0.5 A cm^{-2}. After, the electrode was operating intermittently in intervals of 15 min at 0.5 A·cm^{-2} and 15 min at OCV. During the intermittent operation, the temperature was kept constant at 70 ^{o}C. The following tests were made after 1 week, 2 weeks and 3 weeks. Regularly some distilled water was added to the 30 % KOH bath because of water evaporation due to the high temperature. Some KOH may also have escaped through the faults existing in the bench but it is believed that the concentration didn´t change significantly.

3.5.2. Under-potential deposition (UPD)

The potential window for UPD tests was varied to find the appropriate range for the study. It was selected the range of 0.5 V and 1.7 V to include the silver oxides reduction and the OER. With the objective of obtaining acceptable peak resolutions, the scan rate was varied and a scan rate of 50 $mV.s^{-1}$ was found adequate. The electrode used for the test was one coated electrode, since it has higher surface as compared to an uncoated Ni substrate. A cathode tested before for long term operation in this work was used for UPD, sample T17.003. Before the UPD test a CV scan to the sample was made in the desired window range and slew rate in a 30 % KOH bath a 70 ^{o}C. This test was called background test. After, the sample and the sample holder were immersed in a 30 % KOH bath at 70 ^{o}C containing 11.72 g $AgNO_3$ per liter of solution of 30 % KOH. This is equivalent to a concentration of Ag of 0.046 mol of $Ag{\cdot}L^{-1}$ solution. This value was based in a previous test made in DLR by Li Wang et al [31]. After this test, the bath concentration was changed, to see the effect and the concentration of Ag of 0.054 and 0.058 were used. In the phase diagram, Figure 34, the operating conditions for the present work are at pH of around 13. In this condition, because the pH is so high, most of the Ag is immediately oxidized due to the high alkaline KOH bath. Three CV scans were made to obtain reproducible results that give precision to the test. To avoid RHE deactivation by Ag deposition on the electrode, the set-up in Figure 7 was used. During measurement, a salt bridge prevents the reference electrode from being contaminated by the media.

Figure 7 – Illustration of the set-up used for the RE in the UPD tests.

4. Results and discussion

4.1. Cathodes analysis

4.1.1. Physical characterization

The SEM images of the Ni steel punched metal sheet coated with NiAlMo (39/44/17 wt %) powders in a geometric area of 4 cm^2 using APS are illustrated in Figure 8. SEM images of NiAlMo powders used can be seen in Figure 35, Appendix B. The pictures in the left side of Figure 8 are the as-sprayed samples and the ones in right side are the corresponding leached samples. A variation on the APS parameters, as shown in Table 1, gives rise to differences on the coating microstructure that will be analysed in the following pages. The Al leaching of the coating, in order to increase the porosity, was made as explained in chapter 3.5.1, in a 30 % KOH + 10 % K-Na-tartrate-tetrahydrate solution (complex-former), at 80 ^oC for 24 h. The as-sprayed samples show a clear increase of porosity and thickness and a decrease in the lamellar structure from T17.001 to T17.005. The change in the current applied in APS changed the plasma jet velocity, which increases from T17.001, 239 ms^{-1}, to T17.005, 580 $m{\cdot}s^{-1}$. The velocity changes the exposure time of the particles to the plasma gases thus the exposure to oxygen. As the temperature is above the melting point of the alloy, 1400 ^oC to 1640 ^oC, the different velocity of the cooling down process can create differences in the alloy structure and composition [18]. The relative amount of gases also changes for different samples, almost in a linear way. The plasma spray for sample T17.001 had 40 NLpM of Ar and 3 NLpM of H_2 and for sample T17.005 had 120 NLpM of Ar and 5 NlpM of H_2. As a result of the increase in the H_2 amount the power net in the jet increases. The temperature does not change significantly between samples and remains above the melting point of the alloy. It is possible to say that an increase in velocity and power of the plasma jet creates a decrease in the lamellar structure and an increase of density of the coating, i. e. increase of thickness. In the leached samples, it is possible to see also that an increase in surface area occurs.

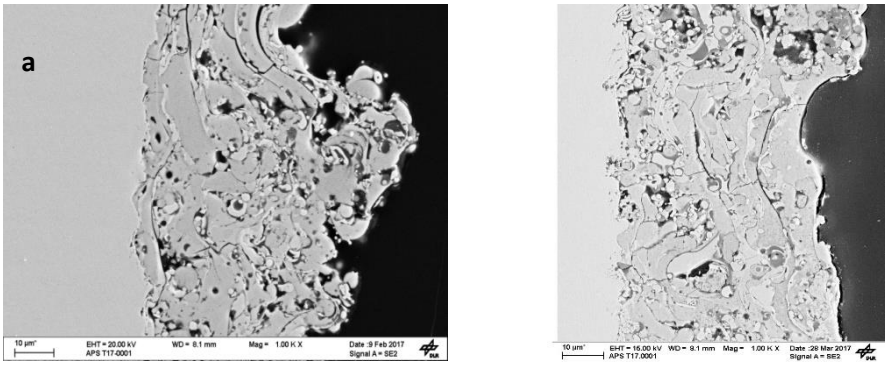

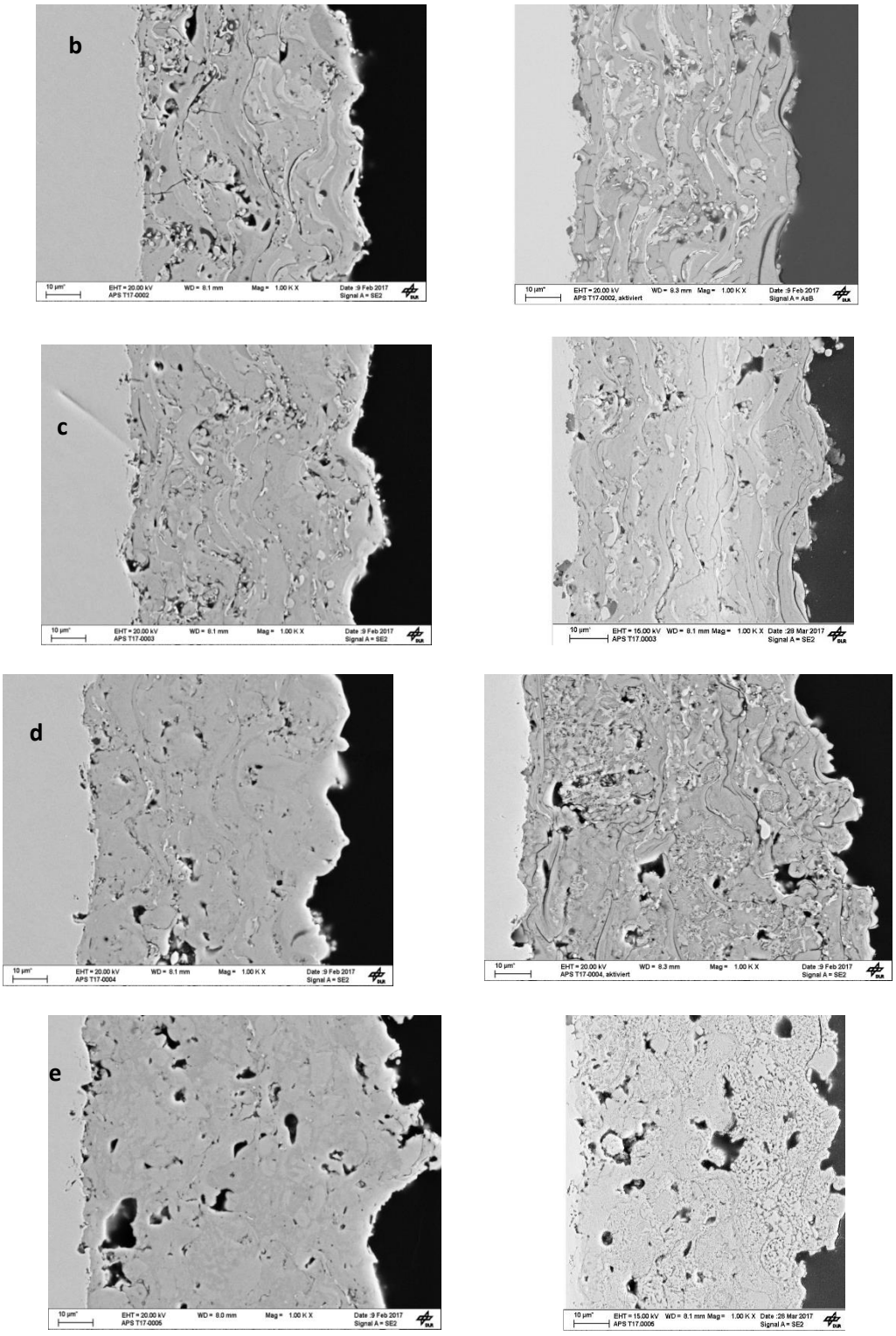

Figure 8 – SEM images of APS as-sprayed samples, in the left, and APS leached samples, in the right: a) T17.001; b) T17.002; c) T17.003; d) T17.004; e) T17.005.

Because the speed of the plasma jet is different, also the exposure times to the plasma that particles experience is different. Lower exposure time creates a layer with less oxygen content in the surface

of as-spayed samples, as seen in Table 4. It could, also, result in less molten particles, but this is compensated by the increase in H_2 content in the plasma jet. The increase of H_2 amount in the plasma spray increases the heat transfer to the particles.

Table 4 - EDX measurements results showing the weight percentage composition of as-sprayed Ni cathodes coated with NiAlMo with different conditions of APS.

wt%	O (%)	Al (%)	Ni (%)	Mo (%)
T17.001	5.94	28.47	45.98	16.61
T17.002	4.09	32.3	45.25	18.36
T17.003	3.20	35.58	43.78	17.44
T17.004	2.15	37.44	44.04	16.37
T17.005	2.01	37.41	44.36	16.22

Besides protecting the particle from oxidation, increasing velocity flattens the particles against the substrate creating a more homogeneous and thus a better cohesive coating. It is possible to see that the homogeneity of the samples increases from sample T17.001 to T17.005. Except for sample T17.005, is possible to distinguish particles in the coating which were not well molten. These particles look similar to the ones shown in the SEM images of the particles in Appendix C, Figure 35. The linear scan of sample T17.001 was made and it is represented in Figure 36.

In all coatings, it is possible to distinguish layers of coating, although it is more obvious for sample T17.001 and less for sample T17.005. The gaps that exist between layers create instability and are responsible for the coating detachment. The gaps are smaller as the velocity of the plasma jet increases. In sample T17.005 the layers can hardly be seen.

Figure 8 shows the leached samples with significantly larger area than the as-sprayed samples. The increase in surface area results from the selective dissolution of aluminium. In Figure 3 the NiAl phase diagram shows that for a 44 % of Al mixture Ni_2Al_3 is formed during the cooling down of the alloy. According to the XRD measurements, Figure 9, in the particles of the alloy coexists NiAl, Ni_2Al_3 and NiAlMo. The Al leaching process leads to the formation of vacancies in the Ni_2Al_3 lattice and aluminium-deficient regions in the particle. As the aluminium content decreases, the Ni_2Al_3 collapses and transforms by short order rearrangement from a fcc structure into an intermediate bcc porous structure [32]. The leaching is more efficient as the surface area increases because more Al can be leached. The increase in surface area before leaching can be a result of different oxidization state of the surface due to different time exposure to the plasma jet. Some AlO is formed during the plasma

spray and the Al in the AlO will not be leached since it is resistant to alkaline corrosion. Therefore, deactivates the area underneath it.

The content in Al is bigger for sample T17.001, as seen in Table 5, due to bigger exposure time during the coating process and therefore more oxidized surface. More Al content is an indication of more AlO and then less Al was leached and after leaching the surface area was lower than the other cathodes.

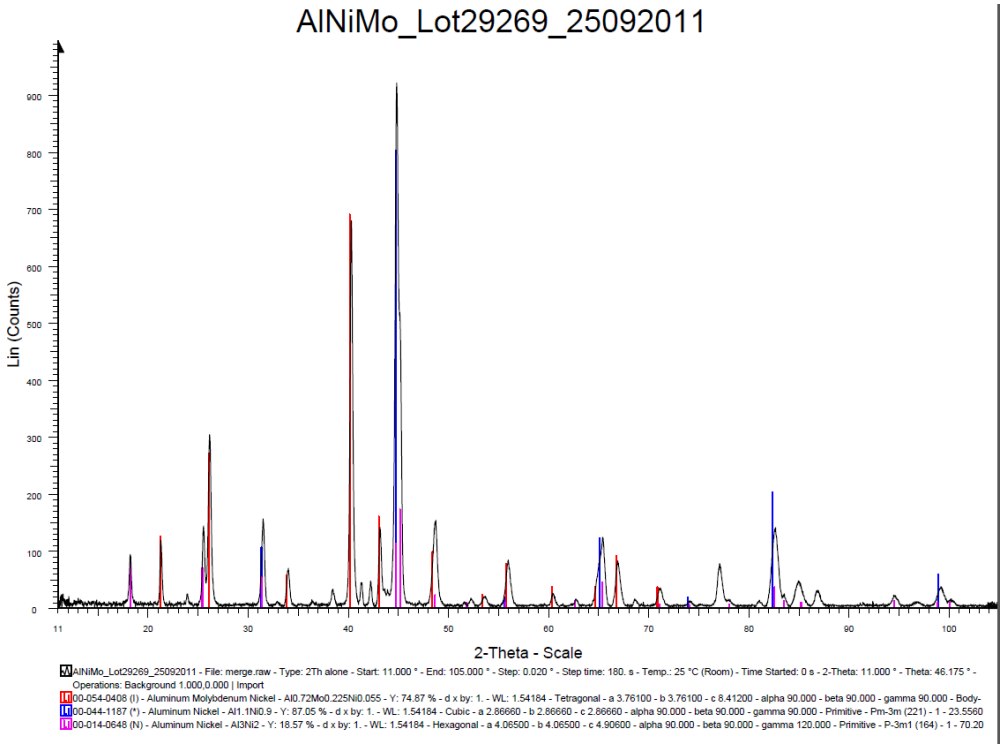

Figure 9 – XRD measurement of the NiAlMo powder.

In Table 5 is also possible to see that the amount of O increases from T17.001 to T17.005. The increase may indicate an increase of surface area. During the leaching, OH^- ions are adsorbed by Ni meaning that in a bigger surface area more $Ni(OH)_2$ can be formed. In order to see the elemental distribution in the coating, the EDX images of samples T17.001, T17.003 and T17.005 are presented in Appendix C, Figure 37. The O present in the Al areas indicates the presence of AlO which prevents a good leaching necessary to give an increase in surface area. As expected from SEM analysis, it is also possible to verify that there are some Al and Mo particles that were not melted in the first two samples. The presence of Mo well dispersed increases the surface roughness which contributes to a bigger surface area [22].

Table 5 – EDX measurements results showing the weight percentage composition of leached Ni cathodes coated with NiAlMo with different conditions of APS.

wt%	O (%)	Al (%)	Ni (%)	Mo (%)
T17.001	10.91	20.77	52.77	13.91
T17.002	14.36	17.39	55.61	10.70
T17.003	16.09	15.92	57.23	8.77
T17.004	17.34	12.27	60.60	6.89
T17.005	18.35	12.70	56.71	10.04

4.1.2. Study of overpotential reduction

In order to compare the potential for HER of the samples, the first day test is represented in Figure 10. A test with an uncoated Ni steel punched metal sheet electrode was also done, in the same conditions to make a comparison with coated cathodes. As explained in section 3.4.1, the cyclic voltammograms were performed at 70 ^{o}C in a 30 % KOH bath, with a slew rate of 5 mV·s^{-1}. The CV show at what potential the HER occurs and if other chemical activity is occurring during the tests. In Figure 10 is only represented the third cycle for each cathode because there is no significant difference between first, second and third cycle so it is possible to assume that the sample has a stable behaviour after only 3 cycles. The cyclic voltammograms were made with the IR-corrected values of potential, calculated by equation 16 using the measured impedance values in Table 7.

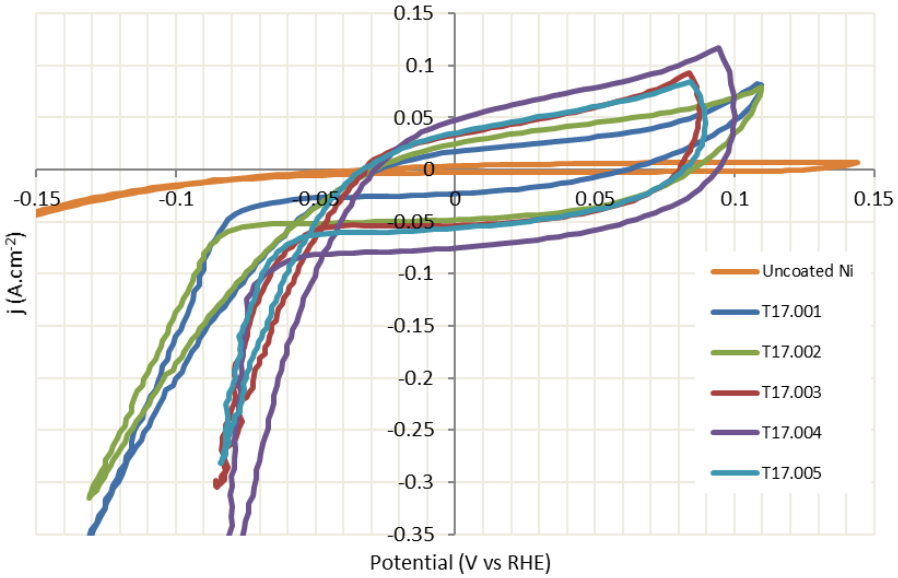

Figure 10 – IR-corrected cyclic voltammograms for Ni electrode coated with Raney-nickel NiAlMo versus uncoated Ni electrode, in 30 % KOH solution at 5 mV·s^{-1} and 70 ^{o}C for the 3rd cycle. Samples T17.001, low plasma jet velocity to sample T17-005, high plasma jet velocity. The correction was made with the impedance values in Table 7.

The scan started in the lower potential, at -0.1 V, was changed until 0.1 V and back to -0.1 V. The increase in cathodic current at negative values of potential is a result for the HER evolution and H_2 formation. The potential at which the HER takes place is clearly lower for the coated cathodes than for the uncoated Ni, represented by the orange line. In this first test, the lowest voltage for HER is shown by T17.004. The slightly increase in the anodic current, in the positive side of yy axis in the reverse scan is due to H incorporation in the Ni surface, which leads to NiH_x formation [14]. A protective film of NiH_x exists, since the HER happens for more negative potentials after the cycle than in the forward scan. The current density is seen to drop quickly when the scan changes from the forward scan to the reverse scan which means that the reduction of NiH_x happens immediately. The symmetrical cathodic and anodic areas can be correlated with a very reversible reaction. Figure 39, Appendix D, intends to clarify where and which changes take place during the cyclic voltammetry. The slope of the curve in the forward scan can be an indication of the rate of the adsorption process, which is limited by solid state diffusion of H to the surface. Therefore, a bigger slope can be an evidence of faster diffusion due to a larger surface area. The similar curves between cycles in Appendix D, Figure 38, indicate that everything that is oxidized is reduced back. The area inside the curves is proportional to the surface area of the electrodes since if more area is available, more NiH_x is adsorbed and the current is bigger. In this first test, sample T17.004 presents the biggest surface area and T17.001 the smallest. Another important factor in the electrochemical activity of the electrode is the presence of Al_2O_3 layer which is corrosion resistant. This oxide layer deactivates the surface area available for adsorption and can be one of the reasons why sample T17.001 has the smallest overpotential reduction and the lowest area. This statement is according with the EDX measurements where it is possible to see that the Al amount is bigger for this sample.

The IR-corrected current-potential curves, corrected using equation 16, and the values of impedance in Table 7 are presented in Figure 11. The values were corrected because different sample holders were used that have different ohmic resistances. The i-V curves result of a potentiostatic scan as described in section 3.5.2. As justified before, the lowest potential of the coated electrodes for HER occurs using sample T17.004 and for highest using sample T17.001. i-V curves give an easier understanding of the electrode performance, although do not show if other reactions are taking place on the electrode that can be the reason for good or bad performances.

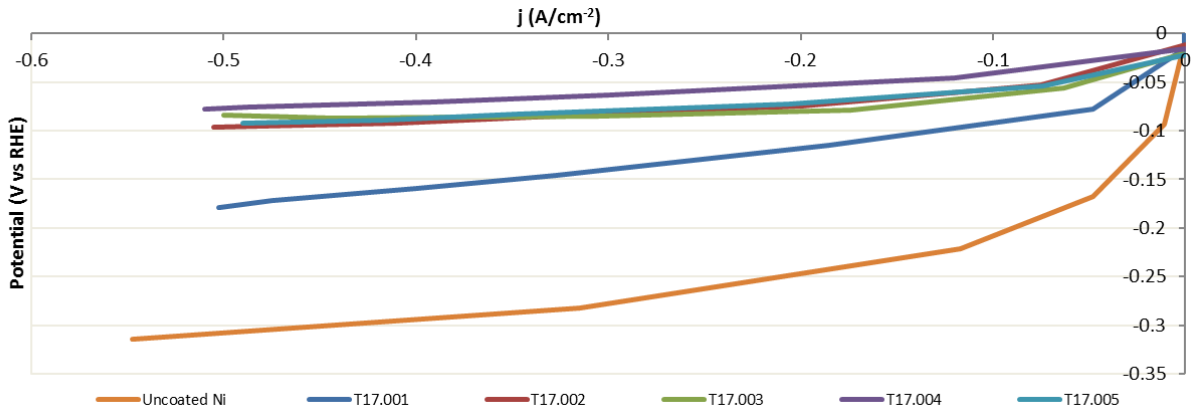

Figure 11 – IR-corrected values of current-potential curves for Ni electrode coated with Raney-nickel NiAlMo versus uncoated Ni electrode, in 30 % KOH solution and 70 ^{o}C on the first day operation; samples T17.001, lowest velocity plasma jet to T17.005, highest velocity plasma jet. The correction was made using equation 16 and the impedance values in Table 7.

The IR-corrected HER potential values of the Ni coated with Raney-nickel NiAlMo versus the uncoated Ni electrode are summarized in Table 6 for each sample, at 0.5 A·cm^{-2} and 70 ^{o}C in a 30 % KOH bath. Also, a reduction compared with the value for uncoated Ni in the same conditions is done.

Table 6 – Electrochemical results at 0.5 A·cm^{-2} in a 30 % KOH bath for the NiAlMo coatings and the potential reduction versus the uncoated Ni sample. Sample T17.001, lowest plasma jet velocity to T17.005, highest plasma jet velocity. It was decided to make the reduction a positive value since benefits HER. The potential is then, less negative than an uncoated electrode.

	Potential (V)	**Reduction (V)**
Ni	-0.314	
T17.001	-0.162	0.153
T17.002	-0.930	0.222
T17.003	-0.084	0.231
T17.004	-0.079	0.235
T17.005	-0.089	0.226

Table 7 presents the impedance measured for all the electrodes in all tests that was used to make the IR corrections of the voltage. These corrections allow to discount the ohmic resistance created by the sample holder, the resistance between the surface of the sample and the position where the RE is connected, and the resistance in the cables but also disregard resistances that give important information about the electrode. The important removed resistances are created by the gas bubbles that forms in the surface of the electrode, the one created by the KOH concentration, by the gas bubbles contained in the KOH solution and by some surface changes of structure or composition. The

temperature was kept constant around 70 ^{o}C so that the variation of resistance with the temperature may not have significant effect in these experiments. For that reason, the values of impedance are listed in this work. It is believed that the main reason for the big difference in impedance between samples and, sometimes in the same sample in different days, is the usage of different electrode holders which have different ohmic resistances. This statement is based in the fact that the impedance should not change to much, considering that the parameters listed above do not change significantly between samples and even less along time in the same sample. In the beginning of the experiments, it wasn't known that the electrode holders had such a different ohmic resistance.

Table 7 – Average impedance resistance measured during the potentiostatic tests used to calculate the iR corrected values for all the Ni electrodes coated with Raney-nickel NiAlMo samples.

mΩ	T17.001	T17.002	T17.003	T17.004	T17.005
1st day	118	164	175	117	191
2nd day	117	157	165	114	156
11th day	114	167	166	118	150
33rd day	114	165	117	114	183
42nd day	167	-	169	165	114

4.1.3. Study of layer stability

The overpotential evolution over time carried out at open-cell voltage (OCV) of the Ni electrodes coated with Raney-nickel NiAlMo at room temperature is shown in Figure 12. The moment when started the loss of coating is represented by the dots. The tests were made at 70 ^{o}C in a 30 % KOH bath and 0.5 A·cm^{-2}.

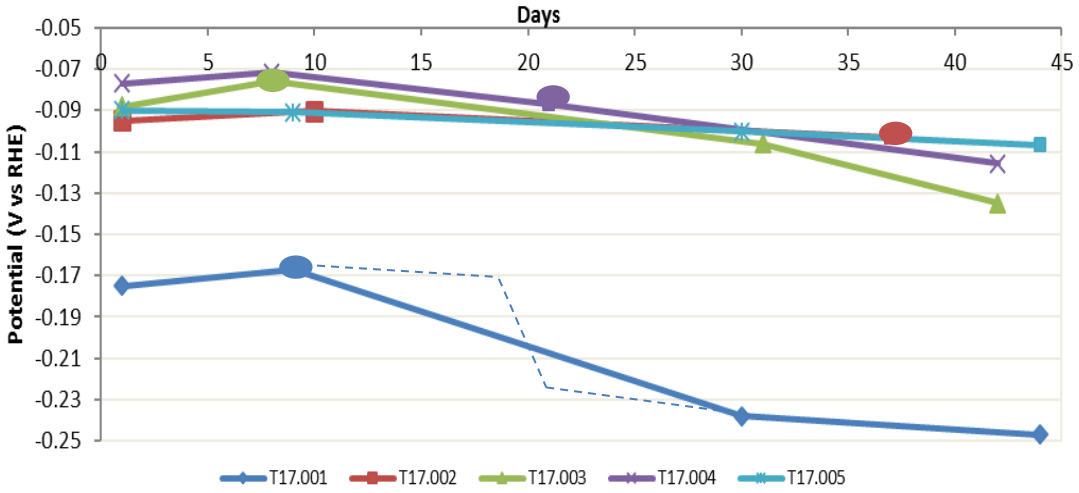

Figure 12 – IR-corrected potential-time dependence of the Ni coated with Raney-nickel NiAlMo in 30 % KOH solution, at 70 ^{o}C and 0.5 A·cm^{-2} after aging at open cell voltage at room temperature. Samples T17.001, lowest plasma jet velocity to T17.005, highest plasma jet velocity. The different coloured big marks represent when it was observed that the coating started to detach. The dashed line represents the electrochemical behaviour shown if more tests were done to the sample.

Figure 12 shows that sample T17.001 lost most of its coating between the first and third week. In the third week, almost all coating was detached. No tests were made in between but it is believed that the actual performance of the electrode changed as described by the dashed line. This sample is the least stable and presents the worst performance. Sample T17.005 is the most stable and until the last test showed no signs of physical degradation. A more detailed analysis of the performance of each electrode over time is shown in Appendix D, Figure 38. In those cyclic voltammograms it is possible to see that after long time tests a small peak starts to appear in the anodic scan. According to the literature, the peak can be attributed to Mo oxidation [21]. This peak can be seen after the electrochemical activity of Ni decreases because of either loss of coating or deactivation of surface area.

In Figure 38 it is possible to see that the area inside the curve and the slope of the H adsorption are decreasing over time. The loss of coating and the deactivation of the electrode surface with non-reducible NiH_x and NiO because of the exposure to alkaline solution can be the cause for such behaviour.

The instability of the coating is mainly due to the gaps existing between layers. Besides this, after long times in an alkaline solution α-NiH_x transforms into β-NiH_x. The transformation, which is a change in structure, damages the electrode and can contribute for the detachment of the coating [33].

Table 7 shows the impedance evolution over time. It shows that the impedance increases when working at 0.5 A·cm^{-2} and decreases over time at OCV. The significant decrease in impedance for sample T17.005 can be a result of incomplete activation, which continued during the first test.

4.2. Anodes analysis

4.2.1. Physical characterization

4.2.1.1. NiAl Raney-nickel

The SEM image of the leached Ni electrode coated with porous NiAl using APS is shown in Figure 13. The coating was prepared spraying NiAl (54/44 % wt) powders using APS in a Ni expanded metal sheet substrate in a geometric area of 4 cm^2. A SEM image of the powders is shown in Figure 40, Appendix E. The leaching of the coating, in order to increase the porosity, was made as explained in chapter 3.5.1, in a 30 % KOH + 1 0% K-Na-tartrate-tetrahydrate solution, at 80 ^oC for around 24. The activated coating shows a very porous sponge-like structure although with several gaps between layers of coating and numerous particles not properly melted. The weaker bonds between layers and the gaps are the main reason for the instability in the coating. However, it can be seen that the surface area is quite big due to the presence of the microstructures marked in the image in red.

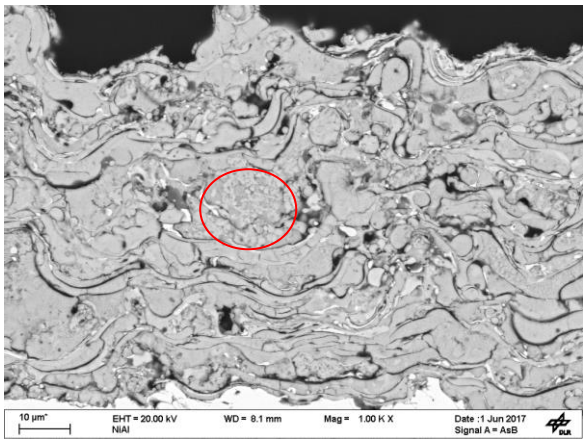

Figure 13 - SEM image of the leached NiAl coating sprayed using APS above a Ni strechmetal electrode; sample T17.025. The marked area shows the microstructure responsible for the surface area increase.

The XRD measurements of the powders are represented in Figure 41, Appendix E, where it is possible to see that both Ni_2Al_3 and Ni_3Al structures were present. Ni_3Al, which is present in bigger amount, is the responsible for the surface area increase after leaching, allowing the growth of the microstructures pointed out with a red circle in Figure 13 [19].

The efficiency of the leaching is confirmed by the EDX measurements, Table 8. The normalized amount of the elements present in the coating, assuming that it is 100 % Ni were also calculated and it is presented in Table 11. The calculations were made dividing the amount of each element by Ni amount and allow the reader to compare the amount of elements in the samples since some of them have big differences in the Ni content. The ratio Al/Ni in the leached sample is around 15/71, as seen in Table 11 The EDX images of the leached coating are shown in Figure 14. It can be seen that some exposed Al, in green, found in the surface and around the gaps, was not leached. This Al may be in

the form of Ni_2Al_3, whose Al is harder to dissolve, or may have been oxidized during APS forming Al_2O_3 which is resistant to KOH corrosion. The presence of Al_2O_3 is confirmed by the light blue colour in the EDX images. The Ni phase is almost depleted of Al what means that it was successfully dissolved in this area. The efficient leaching can be a result of Ni_3Al presence, the Al of which is easier to leach. The great surface area can also be related with the distribution of O in the Ni phase that is confirmed by the great purple area. The presence of O is an indication of extensive OH^- adsorption during the leaching process and formation of $Ni(OH)_2$.

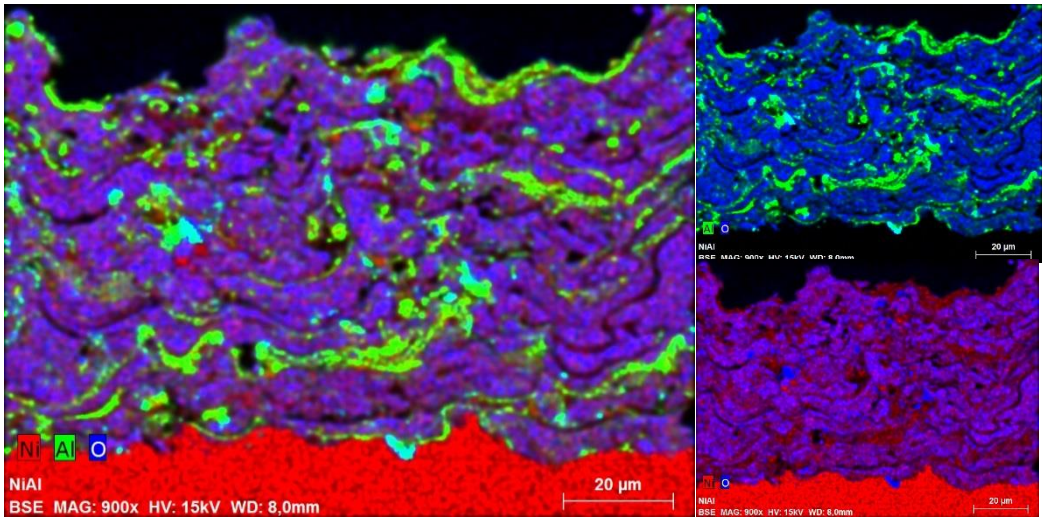

Figure 14 – EDX images of elemental distribution of activated NiAl coating sprayed using APS above a Ni expanded metal sheet substrate; sample T17.025.

Table 8 summarizes the EDX measurement results of all the leached anodes.

Table 8 - EDX measurements results of the composition of leached anodes.

wt %	O	Al	P	Co	Ag	Ni
T17.025.6 NiAl	14.68	14.79	-	-	-	70.53
T17.025.5 NiAl +P	18.16	11.81	0.32			69.31
T17.027 NiAl + Co_3O_4	10.52	21.74	-	25.34		42.40
T17.028 NiAl + Co_3O_4 + Ag	12.91	14.62	-	21.39	25.46	21.39

4.2.1.2. P containing Raney-nickel

Sample T17.025.5, a Ni expanded metal sheet coated with NiAl (54/44 % wt) powders using APS, was treated with P and high temperatures. The addition of P must reduce the surface corrosion and then improve the long-term stability of the electrode. The treatment consisted in spread $H_2NaO_2P{\cdot}H_2O$ in the coated area of the leached electrode and let the reaction take place inside a reactor at high temperature and in an oxygen free atmosphere. The process is explained in detail in chapter 3.3. The SEM image of an activated and shortly operated sample tested immediately after the treatment is shown in Figure 15. The activation procedure is explained in chapter 3.5.1. The test was made in the

same way as the first day tests for the other anodes, i. e. 70 ^{o}C, 30 % KOH bath and CV with the same parameters as the other anodes, as explained in more detail in chapter 3.5.1. The coating looks similar to NiAl coating, very porous, with a lamellar structure and some particles not properly melted. The resemblance with NiAl means that the heat treatment and P addition had no effect in the coating structure, as expected, since the heat treatment reached a maximum of 300 ^{o}C and the melting point of the alloy is between 1400 ^{o}C to 1640 ^{o}C [18].

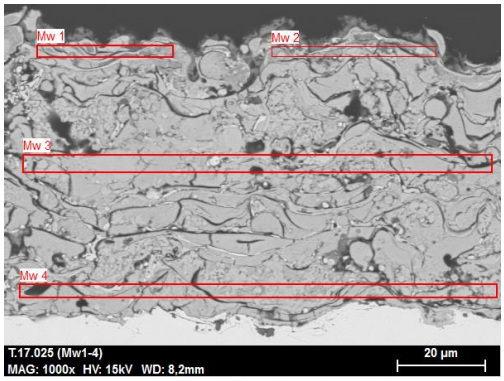

Figure 15 – SEM image of leached NiAl coating treated with P and high temperatures; sample T17.025.5. In red are the analysed areas with EDX whose values are in Table 9.

The original values of the EDX measurements are summarized in Table 8. Table 11 shows the percentage of the elements in this coating normalized by Ni where it is possible to see a big increase of O in this coating towards NiAl. The amount of P, however, must be analysed in different depths of the coating, since the treatment was at the surface. Therefore, another measurement was made in smaller areas at different depths, in the areas shown in Figure 15, whose values are summarized in Table 9. As expected, the amount of P is bigger in the surface than deeper in the coating. An increase in oxygen content towards the sample coated with NiAl was found mainly because high temperatures also promote the oxidation of metals, increasing the content in oxygen. This possible oxidation that occurred during the heat treatment, although it was in a free oxygen atmosphere, can be because of the hypo-phosphide is hydrated [24].

Table 9 – EDX measurement of sample T17.025.5 (NiAl/P coating) after leaching. The measurements were made at different depths, as represented in Figure 23. This table shows the normalized values by Ni amount, assuming that Ni was 100 %.

Wt %	O/Ni	Al/Ni	P/Ni
MW 1	23.86	23.85	4.46
MW 4	26.62	15.00	0.31

A linescan analysis in Figure 42, Appendix E, confirmed how P is distributed inside the coating where can be seen that in the surface there is more P than deeper.

4.2.1.3. Co_3O_4 modified Ni

The microstructures of the Ni strechmetal electrode coated with Co_3O_4/NiAl before and after leaching are illustrated by the SEM images in Figure 16. The activation procedure is explained in section 3.5 and the composition of the coating is described in Table 2. The SEM images were made using different parameters which resulted in different contrast. In the as-sprayed sample, as in the coatings before, it is possible to distinguish different phases made of different materials which are a result of poor melting and poor mixture during the spraying process. This coating is, however, thinner than the NiAl coating which can be a result of poor melting and then poor attachment of the Co_3O_4 to the surface. Layers are easily identified with big gaps between them and the weak bonds between the layers create instability in the coating. After leaching, the porosity did not increase as much as in NiAl coating, and the microstructures pointed out in red for NiAl, in Figure 13, which are responsible for the area increase, also do not appear. Together with the fact that the coating thickness did not decreased significantly after the leaching, it is possible to assume from these images that the activation was not very effective. The poor leaching can also be proved by the EDX measurements in Table 8, where it is shown that the amount of Al is 21 %, the biggest of all the samples.

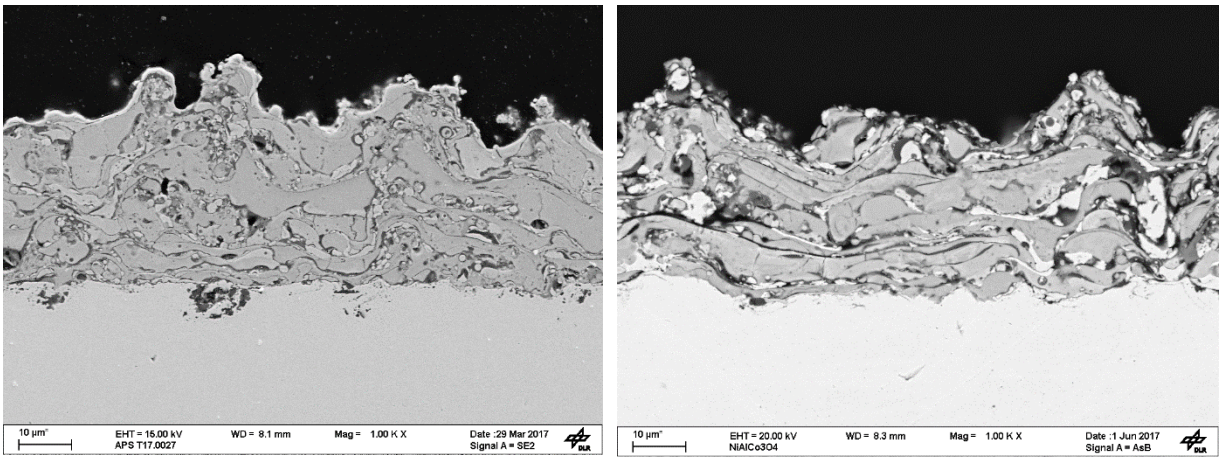

Figure 16 - SEM images of as-sprayed (left) and leached (right) Ni strechmetal coated with Co_3O_4/NiAl using APS. Sample T17.027.

In Figure 17, a comparison between the as-sprayed (left) and activated (right) Co_3O_4/NiAl sample is made based on the elemental distribution. The non-melted particles are easily identified by the primary colours in all the images. The Co_3O_4 is not mixed with Ni as seen in Figure 17 b which creates different phases for OER. While Co_3O_4 improves the current density for OER, NiAl should provide a large surface area for the reaction to take place, also catalysing the reaction. Before leaching, the Ni phase is absent of O, Figure 17 c, but after activation some purple areas resulting of the Ni (red) and O (blue) superposition appear, Figure 17 d. The presence of O in the Ni phase can indicate the area

available for OH^- adsorption. However, this area is small compared with NiAl coating and several areas with Al can be found mixed with Ni in the leached sample what means that the leaching was not efficient, as can be seen in Figure 17 f. O can also be found in Co_3O_4, light blue in Figure 17 a and Al_2O_3, light blue in Figure 17 g. The presence of Co_3O_4 may prevent a good leaching of the coating since the O from Co_3O_4 reacts with Al and oxidises it, avoiding the Al dissolution. This can be seen in the EDX images, because in the as-sprayed samples the areas with Co also have O, and in the activated samples it can be found areas with Co that are free of O. Figure 17 g shows several areas in light blue which are a result of the superposition of Al (green) with O (dark blue).

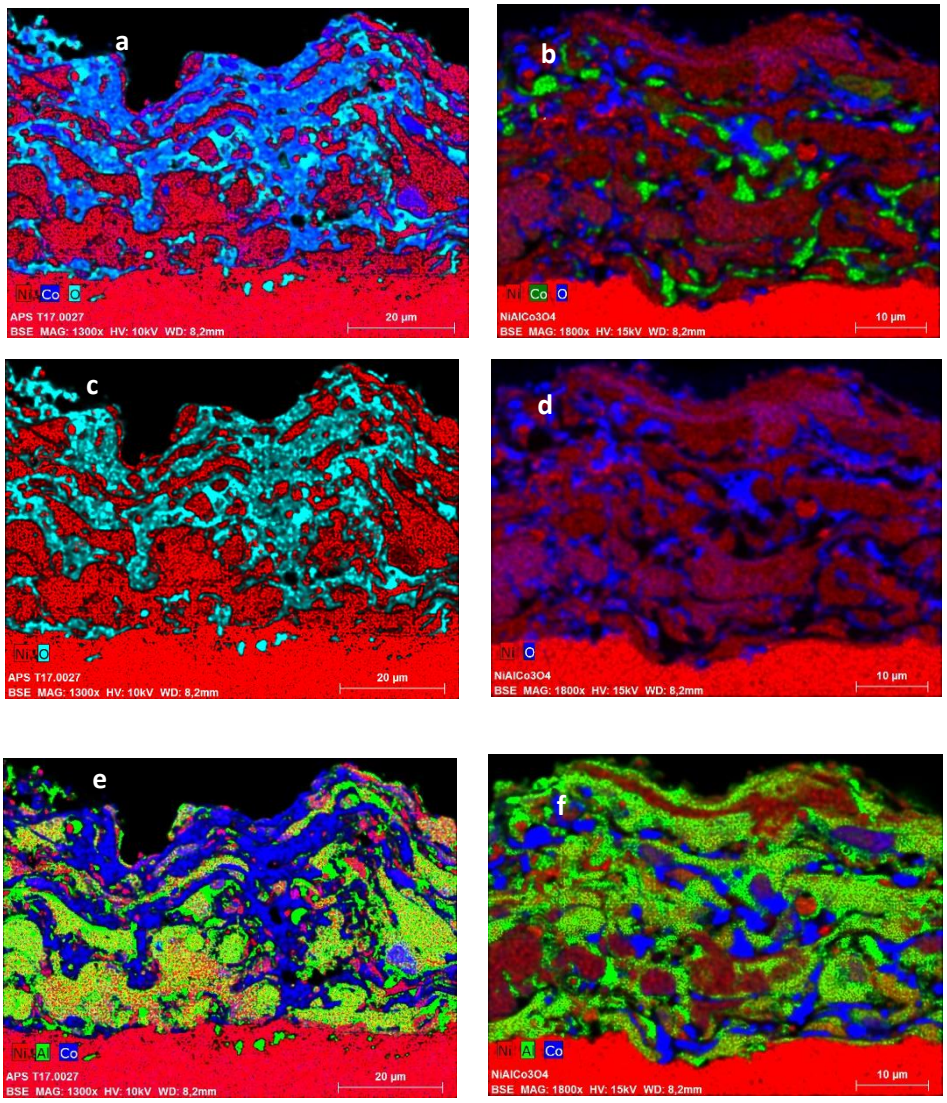

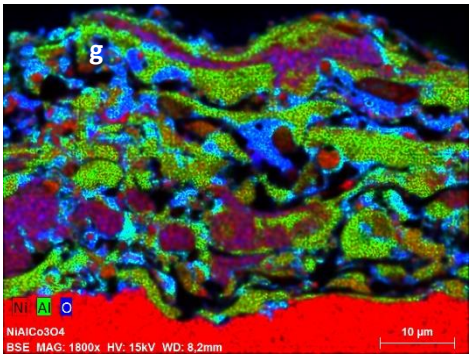

Figure 17 - EDX images of elemental distribution of as-sprayed (left) and activated (right) Ni strechmetal coated with Co_3O_4/NiAl using APS. Sample T17.027.

4.2.1.4. Ag/Co_3O_4 modified Ni

Figure 18 shows the SEM image of the activated Ni strechmetal coated with Ag/Co_3O_4/NiAl using APS. The activation procedure is explained in section 3.5 and the composition of the alloy is described in Table 2. In this sample is possible to distinguish three different phases, the NiAl phase, the Ag phase and the Co_3O_4 phase. Two ways of catalysing the reaction are present in this coating. Ag/Co_3O_4 is a highly active combination which reached high current densities at low voltage for OER in past studies and the NiAl phase provides a large surface area for the reaction to take place, also catalysing the reaction [27]. The leached coating in Figure 18 is very porous and lamellar with large gaps between the layers. Layers of Ag are easily identified in the SEM image by the white areas which is confirmed by the EDX images, Figure 19, with light blue colour. Although some Ag was corroded during the leaching, because the leaching bath had black particles of silver oxide, some Ag can still be found in the coating. However, as will be seen in the following chapters, the presence of current will promote Ag oxidization and coating destruction. A few particles of powder can also be distinguished in the coating which are the result of poor melting during the spray process. The sample seems to be very unstable due to the weak bonds between layers and due to the large Ag areas.

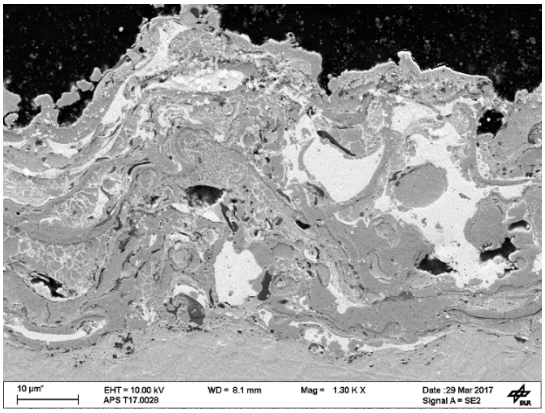

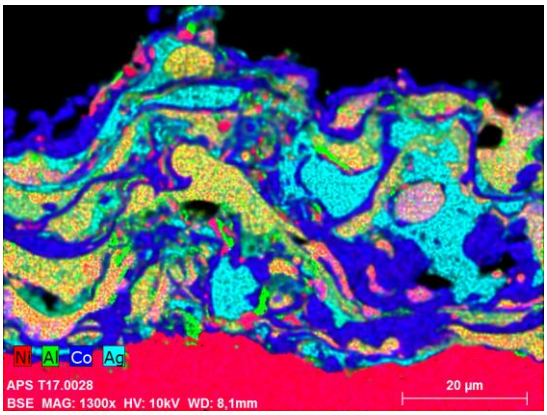

Figure 18 – SEM image of sample T17.028 leached (with silver) Figure 19 - EDX images for Ag/Co_3O_4 Ni-containing electrode.

The elemental distribution of all the elements in the coating is shown in Figure 19 and more detailed maps are shown in Figure 43, Appendix E. The magenta colour in Figure 19 stands for the Ni (red) and Co (blue) mixture and the yellow stands for Ni (red) and Al (green) phase. The large NiAl surface means that the leaching was not effective which can be because of the strong oxidation of Ag during leaching that used the KOH available. After 24h in leaching solution, at 80 ^{o}C, the bath was full of small black particles which mean that silver oxide, was formed and dissolved. According to the ratio of the EDX measurements, summarized in Table 11, this sample has a very high amount of O and Al in comparison to Ni, although it has also the lowest amount of Ni because half of NiAl was replaced by Ag. O is concentrated in Co_3O_4 form and formed also an aluminium oxide and hydroxide. The presence of Ag and Co benefits OER evolution, even though the surface area is not as large in the other samples.

4.2.2. Study of overpotential reduction

In order to compare the potential for OER of the samples, the first day test is represented in Figure 20. As explained in section 3.5.1, three cyclic voltammograms were performed at 70 ^{o}C in a 30 % KOH bath, with a slew rate of 5 mV·s^{-1}. In Figure 20 it is only represented the third cycle for each anode since for most samples the performance does not change significantly from the first cycle to the third. For sample T17.028, Ag-containing coating, there is a clear decrease in the charge of the cathodic peak as the number of cycles increase which is shown in Figure 24. The cyclic voltammograms were made with the corrected voltage calculated by Equation 16 using the measured impedance values in Table 12.

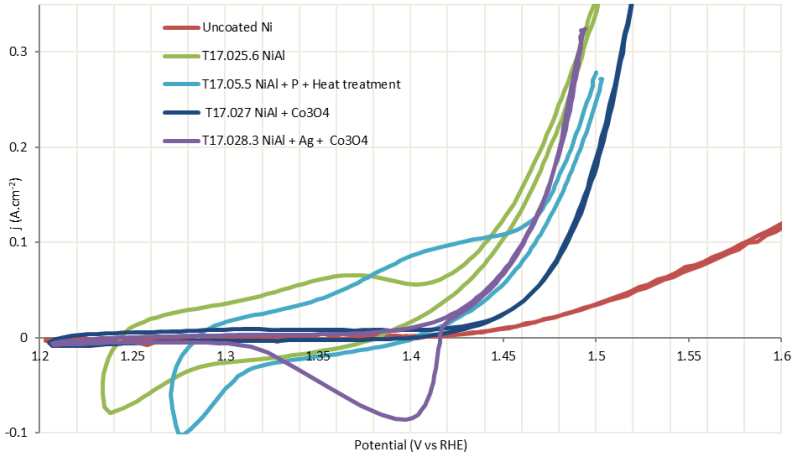

Figure 20 – IR-corrected cyclic voltammograms for coated Ni anodes versus uncoated sand blasted Ni electrode, in 30 % KOH solution at 5 mV·s^{-1} and 70 ^{o}C for the 3rd cycle.

The broad area inside the CVs of samples with NiAl (T17.025) is an indication of a large active area. The adsorptions and desorptions taking place on the surface increase suggestively the current density. NiAl coating was an effective catalyst due to the large surface area for OER evolution.

The sample treated with P and high temperature had no structural changes, so the surface area is similar to the sample coated with Raney-nickel NiAl, as seen in the SEM images (Figure 15). Nevertheless, this sample presents higher potential for OER and the NiOOH peak moved to higher voltage values. A test with a sample only submitted to heat treatment, without P, was made and in the first day, this sample presented the same behaviour as the sample with P. This can be an indication of the oxidation of the surface because of the high temperature treatment which promote the oxidation by the oxygen from the hydrated hypo-phosphide [24]. Surface oxidized Ni anode is less active than Ni anode because of electronic resistance of surface oxide, so OER happens for higher potential.

For the two NiAl samples, the electrochemical activity increase before the OER, represented as a peak in the CV around 1.4 V, is a result of NiOOH formation according to Equation 14. A cathodic peak starts to appear around 1.3 V in the reverse scan which can be due to the NiOOH reduction back to $Ni(OH)_2$. The reduction is not complete, and a permanent film of NiOOH may be created.

The sample with Co_3O_4 has a very small surface area when compared with NiAl samples which can be a result of poor leaching. This statement is according to the SEM images in Figure 16 that show low porosity and to the EDX images, Figure 17, that show a great amount of Al. The lack of a peak for NiOOH also accounts for the low surface area available for the adsorption to take place. Because the reaction did not happen in a large extent on the Ni surface, the peak did not appear. In this case, the OER cannot be favoured by the great surface area so the significant increase on OER voltage towards sand blasted uncoated Ni electrode is because of the good catalytic activity of Co_3O_4.

After the activation of sample T17.028, the bath was found full of black particles in it. Because the particles were black, it was assumed that it was silver oxide [27] [34] [35]. The oxidation of Ag happened during the leaching because the OH^- adsorbed in the Ni surface reacted with Ag forming $Ag(OH)_2^-$ which is high soluble leaving the coating, according to Equation 19 and 20 [27] [34].

$$\mathrm{Ag} + \mathrm{OH}^- \longrightarrow [\mathrm{Ag(OH)_2}]^-_{\mathrm{ads}} + \mathrm{e}^- \quad (19)$$

$$[\mathrm{Ag(OH)_2}]^-_{\mathrm{ads}} \longrightarrow [\mathrm{Ag(OH)_2}]^-_{\mathrm{aq}} \quad (20)$$

However, the formation of $Ag(OH)_2^-$ does not give appreciable amounts due to the favourable energetics for the following reaction [34]:

$$2\mathrm{AgOH} \longrightarrow \mathrm{Ag_2O} + \mathrm{H_2O} \quad (21)$$

Therefore, the Ag dissolved during leaching creates gaps in the coating that becomes unstable. Because Ag_2O is barely soluble in water, it forms the black particles seen in the leaching bath. The detachment of silver oxides is confirmed in the EDX images, Figure 43, where a coating with low amount of oxygen can be seen. It is believed that different silver oxides are being formed according to equations 23 and 24, Appendix C. $Ag_2O \longrightarrow AgO$ happens during OER. At 1.4 V AgO is reduced to Ag_2O [27]. In the CV scans made, the Ag was never reduced back to metallic Ag since the potential was not low enough. Therefore, no peak for Ag oxidation appears before. The anodic peak for NiOOH $\leftrightarrow$ $Ni(OH)_2$ transformation doesn´t appear and that means that the adsorption in the Ni surface is not happening to an extent possible to be seen in the CV at the slew rate used. The slope for OER is very high what means that the reaction for the oxygen formation happens fast due to the high catalytic activity of Ag and Co_3O_4. Additionally, there is a sudden increase in the current when the OER starts to take place, which is a result of the presence of catalysts. The potential is the lowest for OER since Ag and Co_3O_4 are present because both are highly active catalysts for OER.

The IR-corrected i-V curves were made using potentiostatic measurement, as described in chapter 3.5.2 are represented in Figure 21.

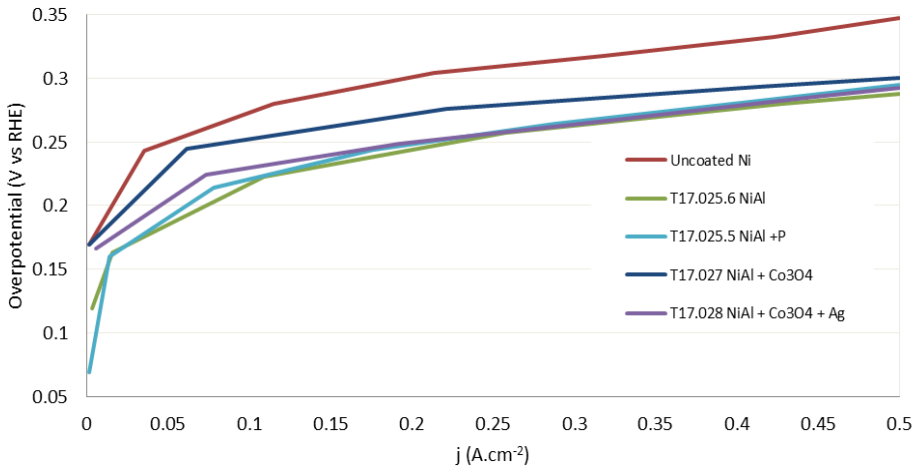

Figure 21 - IR-corrected values of current-potential curves for coated Ni anodes versus uncoated Ni anode, in 30 % KOH solution and 70 ^{o}C on the first day operation. The correction was made using equation 16 and the impedance values in Table 12, Appendix F. The overpotential is a difference of the obtained IR-corrected measurements with 1.23 V [10].

Within the precision and reproducibility of the experiment, estimated as ± 10 mV, the curves for the samples are similar, with some slightly higher voltage at low current densities for T17.027, the sample with Co_3O_4/NiAl. The IR-corrected values of the potential obtained for OER at 0.5 A·cm^{-2}, 70 ^{o}C in 30 % KOH are shown in Table 10 as the voltage reduction of all samples compared with the accepted value of 1.23 V for OER [10].

Table 10 - Electrochemical results at 0.5 A·cm^{-2}, 70 ^{o}C in 30 % KOH for the coated Ni anodes and the overpotential reduction compared with the uncoated Ni sample (1.23 V).

Sample	Potential (V)	Reduction (V)
T17.025.6 NiAl	1.518	0.288
T17.025.5 NiAl +P	1.525	0.295
T17.027 NiAl + Co_3O_4	1.530	0.300
T17.028 NiAl + Co_3O_4 + Ag	1.522	0.292

The measured impedance used to calculate the corrected values of voltage are shown in Table 12. As for the cathodes, the main reason for the difference between impedances is that different sample holders were used.

4.2.3. Study of layer stability

Figure 22 shows the overpotential of OER as function of time for all the electrodes tested. The values represented are IR-corrected voltage using the impedance in Table 12 and were obtained after a potentiostatic test, at 0.5 A·cm^{-2}. Between every test (represented by dots) the samples were operating discontinuously, 15 min at OCV and 15 min at 0.5 A·cm^{-2} in a 30 % KOH bath and a 70 ^{o}C, which is believed to be very stressing conditions for anodes in long term operation. Before the potentiostatic test, all anodes were working around 15 min at 0.5 A·cm^{-2}.

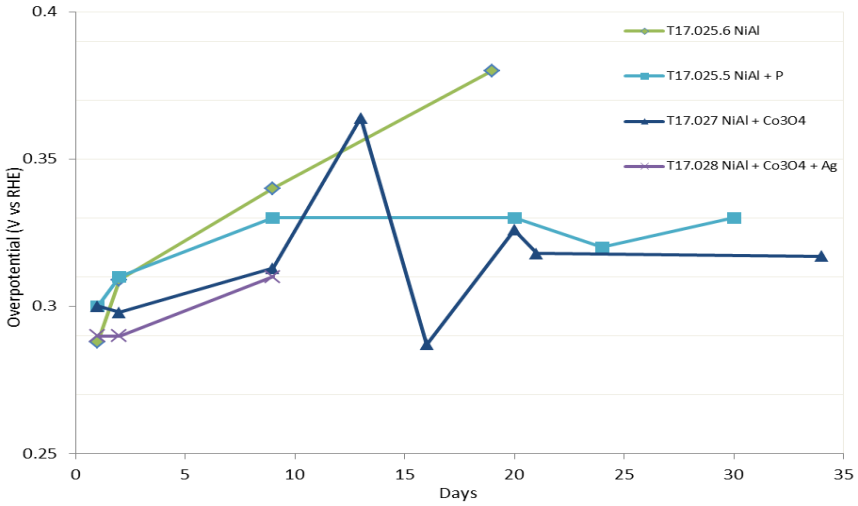

Figure 22 – Corrected values of overpotential-time dependence of the coated Ni anodes in 30 % KOH solution and 70 ^{o}C after aging operating discontinuously in intervals of 15 min at OCV and 15 min at 0.5 A·cm^{-2}.

The most unstable samples were T17.025.6, with NiAl coating, and T17.028, with Ag in the coating.

The NiAl coating detached completely after 20 days which can be justified by the SEM image in Figure 13 that shows a lamellar structure, with weak bonds between layers, several gaps and a few particles not melted. According to literature, repeated cycles creates damages and strains in the coating

structure leading to its detachment due to the transformations of NiOOH ⇌ $Ni(OH)_2$ happening in the surface. In these electrodes, this reaction is identified by an increase in current just before OER, around 1.4 V. In Figure 23 it is possible to see that the charge associated with the anodic peak decreases over time. According to literature, the decrease can be a result of the gradually transformation of α-$Ni(OH)_2$ into β-$Ni(OH)_2$ after long term exposure of Ni to alkaline environments. As the β-phase is more stable, its reduction may happen for more negative potentials which are not achieved in these tests. After long term operation, the OER happens for bigger values of potential which can be a result of coating detachment. Because this β-phase is more stable, its appearance could be beneficial for the electrode, since the redox cycles stop occurring so easily and fewer damages are made [33]. After the first week, the surface area remains stable and eventually the NiOOH peak disappears when a significant amount of coating detaches completely and β-phase is the major phase in the surface. The potential for OER keeps increasing due to the loss of coating although in this test never reached the same potential of the sand blasted Ni sample.

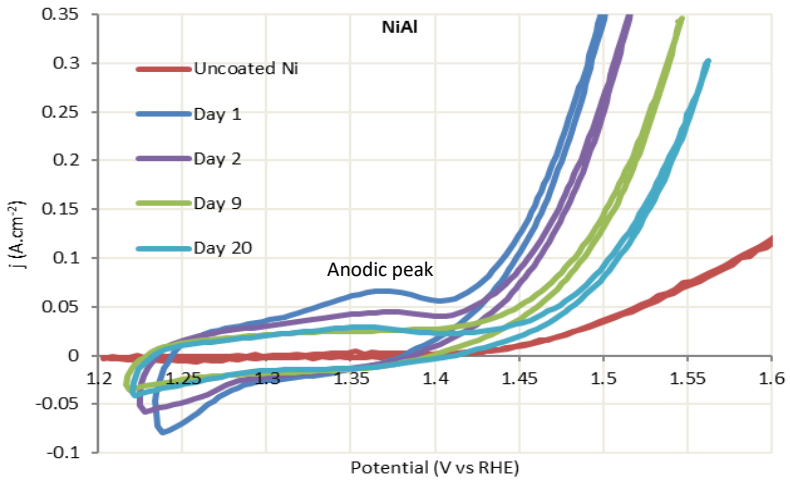

Figure 23 - Cyclic voltammograms for Ni anode coated with NiAl using APS versus uncoated Ni anode, in 30 % KOH solution at 5 $mV \cdot s^{-1}$ and 70 ^{o}C for the 3rd cycle at different times. Long term discontinuous operation at 0.5 $A \cdot cm^{-2}$ for 15 min and 0 CV for 15 min.

Figure 24 shows the evolution of the performance of sample T17.028. After working at 0.5 $A \cdot cm^{-2}$ for 24 h no big decrease in surface area was found, however, in intermittent operation the coating was completely destroyed after 9 days. During the intermittent operation, the OCV condition facilitates silver dissolution according to equations 19 and 20. With increase number of cycle, the intensity of the peak for AgO ⟶ Ag_2O reaction decreases which can be because Ag_2O is slightly soluble in water due to the formation of $Ag(OH)_2^-$. The dissolution of Ag because of its reaction with OH^- creates big gaps and leads to the coating destruction.

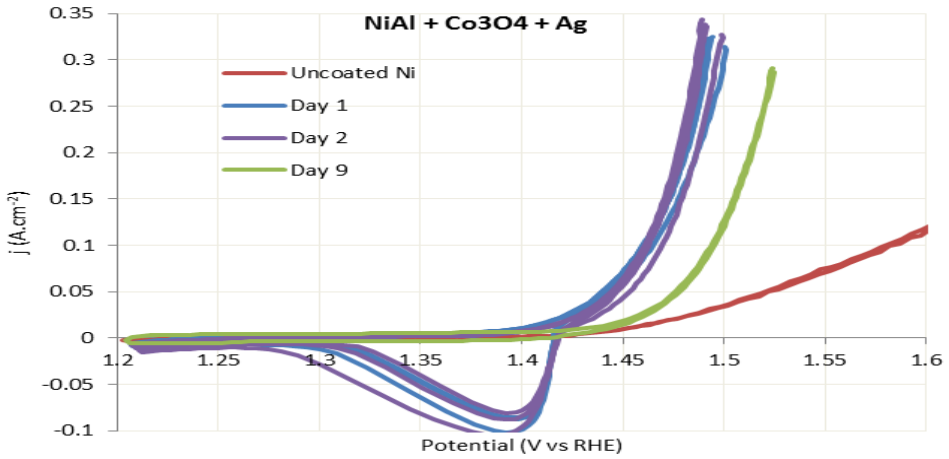

Figure 24 - Cyclic voltammograms for Ni anode coated with Ag/Co_3O_4/NiAl using APS versus uncoated Ni anode, in 30 % KOH solution at 5 mV·s^{-1} and 70 °C for the 3rd cycle at different times. Long term discontinuous operation at 0.5 A·cm^{-2} for 15 min and OCV for 15 min.

Samples with Co_3O_4 and with P seem to be stable since they didn't lose significant coating until the test was stopped. For the P containing sample, the active surface area reduces eventually to the same as the NiAl coated sample. However, the OER potential remains constant. The purpose of adding P is to prevent Ni corrosion and then prevent the coating destruction. In fact, the peak corresponding to the NiOOH ↔ $Ni(OH)_2$ does not exists except for the first test. However, it is not possible to conclude whether the improvement in stability was due to the presence of P or because of the heat treatment. The exposure to high temperatures promotes oxidization, by the water contained in the Hypo-phosphide, and oxidized surfaces are more stable than metallic surfaces, although less chemically active because of electronic resistance of surface oxide [24]. The more stable behaviour may be because NiO does not allow NiOOH ↔ $Ni(OH)_2$ reaction and then protecting the surface against strains [28].

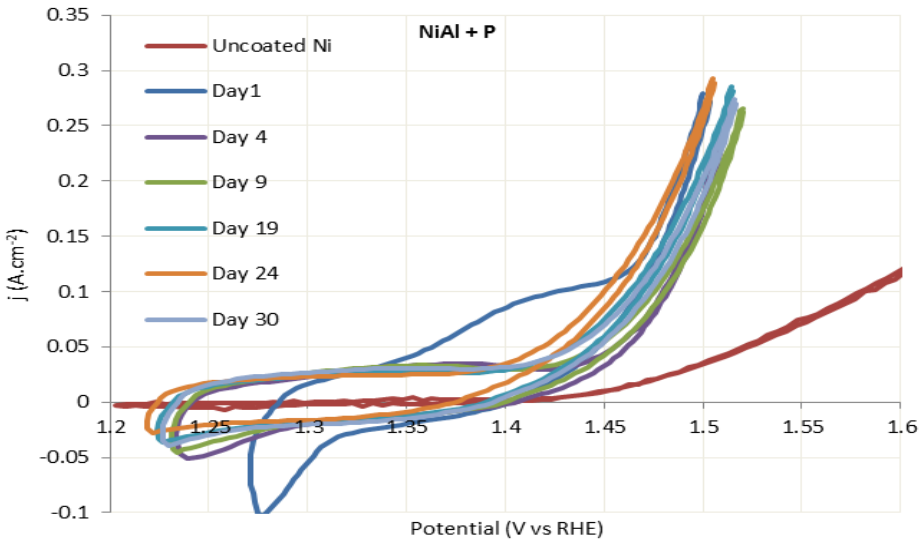

Figure 25 - Cyclic voltammograms for Ni anode coated with P/NiAl using APS versus uncoated Ni anode, in 30 % KOH solution at 5 mV·s^{-1} and 70 °C for the 3rd cycle at different times. Long term discontinuous operation at 0.5 A·cm^{-2} for 15 min and OCV for 15 min.

The coating of sample T17.027 remained stable although with lower electrochemical activity as can be seen in Figure 26. The fact that the coating did not detach can be a result of the contribution of Co to catalyse the OER and then avoiding repeated Ni(II) into Ni(III) transformations. After some cycles, it can be seen in Figure 26 that a peak starts to appear. This peak is believed to be a result of Co oxidation which does not promote the OER since metal oxides have high electronic resistances [24]. The fickle potential of this sample between day 13 and day 16 can be a result of a problem with the device used to control the operation mode of the set-up. A mechanical timer was used to control automatically the intermittent operation which was programmed to operate at 0.5 $A \cdot cm^{-2}$ for 15 min and at OCV for other 15 min. However, the timer failed before the test in the 13th day and when it was fixed, after the 16th day, the voltage went to constant values.

The impedance evolution used to make the IR-corrections of all anodes is described in Table 12, Appendix F. Over time and in discontinuous operation NiAl and NiAl/ P impedances are quite stable, however during the test with the Co_3O_4/NiAl coated electrode, it changes drastically which can be a result of the unpredicted behaviour of the timer.

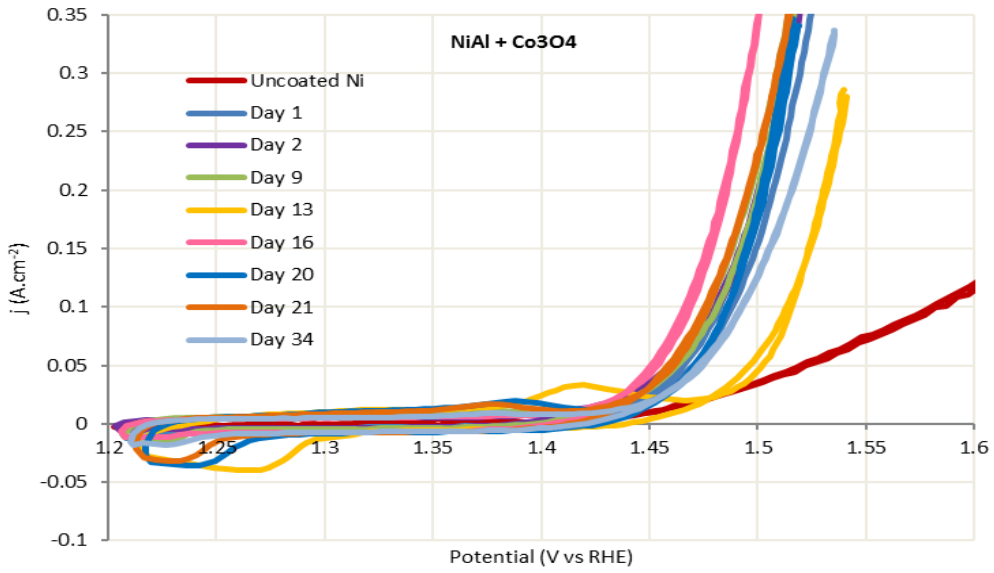

Figure 26 - Cyclic voltammograms for Ni anode coated with Co_3O_4/NiAl using APS versus uncoated Ni anode, in 30 % KOH solution at 5 $mV \cdot s^{-1}$ and 70 ^{o}C for the 3rd cycle at different times. Long term discontinuous operation at 0.5 $A \cdot cm^{-2}$ for 15 min and OCV for 15 min.

4.3. UPD

To test if the under-potential deposition could work in a Ni substrate in alkaline electrolysis, sample T17.003 previously tested as cathode in long term operation was used. Because a coated electrode has a greater surface area than a Ni substrate, the charge associated to Ag deposition is higher and is easier to identify in the CV. Figure 27 shows the CV for the electrode tested in a 30 % KOH bath with 0.046 mol of Ag_2NO_3 per liter of solution and the CV scan of the same electrode in a 30 % KOH without Ag both at 70ºC. The potential started at 1.7 V, point 1, was decreased until 0.5 V, point 2 then reversed until it reaches 1.7 V again. A difference between the CV scan made in the presence of Ag and the CV made without Ag, is clear. The essential features of the blue voltammogram match very well with the reported voltammogram of bulk Ag in Figure 33. The voltammogram for bulk silver is defined by three prominent cathodic peaks that can also be seen here, peaks C3, C2 and C1. After oxygen reduction reaction, starting in point 1, a small increase in the cathodic current can be seen, peak C1. This increase must be a result of reduction of the silver oxidized in the bath that was adsorbed in the surface to a lower state of oxidation. The surface was, at this moment, covered with silver oxide and the peak associated with Ni^{3+} reduction to Ni^{2+} does not appear, as in the red line because the Ni cannot be accessed by OH^-. Peak C3 must correspond to silver reduction to metallic Ag. In the reverse scan, metallic Ag is oxidized in peak A2 forming Ag_2O in the surface of the electrode and A1 is an increase on silver oxidation state, to AgO or Ag_3O_4 [27].

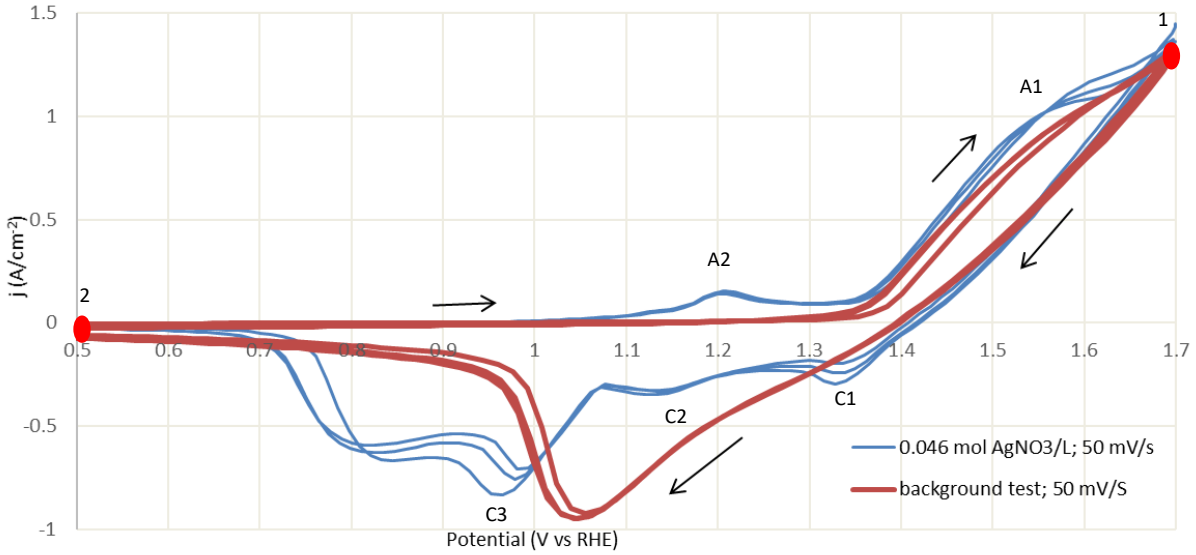

Figure 27 – Cyclic voltammetry scan of a Ni electrode coated with NiAlMo using APS in a 30 % KOH bath at 70 ºC (red line) and in a 30 % KOH bath with 0.046 mol $AgNO_3$ L^{-1} solution (blue line). Both scans were made with a slew rate of 50 $mV \cdot s^{-1}$.

Figure 28 shows another CV scans that shows the effect of changing the concentration of Ag in the bath and the slew rate of the scan. Before the OER the current increases in a peak which can be the oxidation of Ag taking place at the surface of the electrode during OER. A monolayer of silver oxide must be formed in the surface of the electrode. Between curves orange and red, the charge of the peak is the same however, the concentration of Ag in the bath was increased. The fact that the peak has the same charge as before can be an indication of a monolayer formation. Since in the first test it was the monolayer filled all the surface area of the electrode, in the second test, the same number of Ag molecules was adsorbed in the surface forming a monolayer and no more.

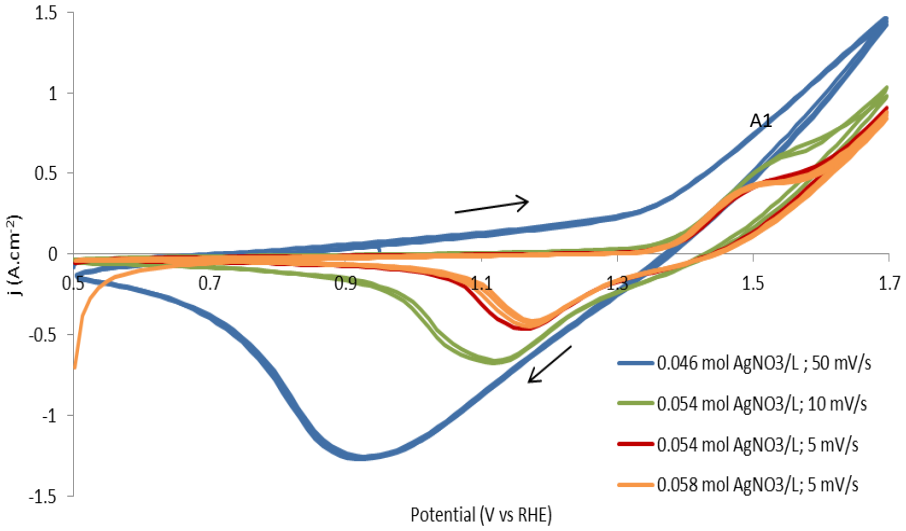

Figure 28 - Cyclic voltammetry scan of a Ni electrode coated with NiAlMo using APS in a 30 % KOH bath at 70 ^{o}C with different amounts of Ag and at different slew rates.

Because of lack of time, no further studies were done. However, the tests indicate that a monolayer of Ag forms in the surface of the electrode, so calculating the charge of the increase in current, it can be possible to calculate the real surface area of the electrode.

5. Assessment of the work done

5.1. Objectives achieved

Ni substrates were coated with NiAlMo using atmospheric plasma spraying to be tested as cathodes. Different plasma jet velocity and composition was used in the spraying to understand how it can influence the stability and the activity of the electrode in alkaline water electrolysis. The stability of cathodes was tested in long term operation at room temperature with no external voltage applied. APS coated electrode with high speed plasma jet at 580 $m.s^{-1}$ was found to have a reduction of 0.226 V in hydrogen evolution reaction that was stable for, at least, 40 days. The higher the speed of the plasma jet used in the coating process, the more stable was the electrode and the higher was its electrochemical activity. It was found that because of the high speed of the plasma jet, the time exposure to the atmosphere was lower, and therefore the oxidation of the particles. Less oxidized particles are more active than oxidized ones because the Al can be more efficiently leached creating a higher surface area to the hydrogen evolution reaction to take place. Moreover, a higher speed jet does not create a lamellar structure, which is more unstable than a homogeneous coating. The increase in H_2 gas in the plasma jet also contributes to the production of a stable coating since the particles of coating are more efficiently melted. APS was found to be able to produce promising coatings if high speed plasma jet and high concentration of H_2 in the plasma jet are used.

Ni substrates were also coated with Raney-nickel NiAl using atmospheric plasma spraying. They were tested as anodes in long term discontinuous operation, changing between OCV and 0.5 $A \cdot cm^{-2}$. An increase of surface area towards uncoated Ni was achieved with porous NiAl, although the coating of this sample was deactivated after 20 days. The instability of the coating was found to be due to the lamellar structure of the coating found in the SEM images. Adding Co_3O_4 to the NiAl coating a decrease of 0.05 V for oxygen evolution compared to uncoated nickel and a stable sample that lasted for 35 days was achieved. Ag mixed with porous NiAl lowered the voltage for oxygen evolution reaction by 0.292 V, although it was very unstable in alkaline environment and the coating was lost after 9 days. Its instability was a result of the extensive corrosion of Ag by KOH. Thus, even if Co_3O_4 did contribute with a high electrochemical activity to the reaction the overall effect would be lower. The addition of P can improve the stability of the coating, however further studies must be done on this subject.

Under-potential deposition of Ag in a Ni electrode was found to be possible to be used as a method to calculate the surface area of the coating. It is assumed a monolayer of silver oxide on the Ni

surface was identified in the cyclic voltammogram scans the charge of which can be calculated and used to estimate the area available for the adsorption.

5.2. Limitation and future work

The biggest limitation of the use of coated electrodes is its low stability after long term operation. It is created by the several transformations that take place in the surface of the electrode as a result of repeated cyclic potential scans. The instability can be prevented by stopping these reactions, which can be done by adding different compounds or giving a very stable structure where strains are difficult to grow. The barriers to hydrogen and oxygen evolution reactions decrease the efficiency of alkaline water electrolysis. Because the controlling step of these reactions is the adsorption in the surface of the electrode, increasing it is a method to decrease the losses of energy and increase the efficiency of the process. Additionally, the addition of more active compounds to these reactions can be made.

The improvements in anodes, in particular, can be done by changing the APS parameters, for coating NiAl, as done for the cathodes in order to achieve a better melting of the particles and achieve higher surface areas. Ag may not be the best option for long term operations because of the extensive reaction of Ag with KOH. Co_3O_4 with NiAl may also not be the best option since the presence of Co_3O_4 prevented a good activation of the NiAl coating. Further tests must be done to understand the role of P in the coating performance, since the improvements were probably because of the heat treatment.

When it comes to the under-potential deposition, further tests must be done. For example, analyse the change in the weight of the electrode at the same time that the cyclic voltammogram is scanned. A better understanding of what is happening in the surface of the electrode can be achieved by using image analysis.

5.3. Final assessment

The overall experience was successful and contributed for a better understanding of the fabrication processes parameters of the electrode that influence its performance in alkaline electrolysis and how its composition can be amend. Based on these discoveries, further work can be done, driving forward the alkaline electrolysis as an efficient method to produce highly pure hydrogen that can be used as an energy carrier in the foreseeable future.

References

[1] Sapountzi, Foteini M., et al., "Electrocatalysts for the generation of hydrogen, oxygen and synthesis gas," *Progress in Energy and Combustion Science,* vol. 58, p. 1–35, 2017.

[2] D. M. F. Santos, C. A. C. Sequeira und J. L. Figueiredo, „Hydrogen production by alkaline water electrolysis," *Química Nova,* Bd. 36, pp. 1176-1193, 2013.

[3] Schalenbach, Maximilian, et.al, "Acidic or Alkaline? Towards a new perspective on the efficiency of water electrolysis," *Journal of The Electrochemical Society,* vol. 163 (11), pp. F3197-F3208, 2016.

[4] Cai, Jing, et al., „Fabrication of three-dimensional nanoporous nickel films with tunable nanoporosity and their excellent electrocatalytic activities for hydrogen evolution reaction," *International Journal of Hydrogen Energy,* Bd. 38, pp. 934-941, 2013.

[5] Schiller, G.; Henne, R. and Borck, V., "Vacuum plasma spraying of high-performance electrodes for alkaline water electrolysis," *Journal of Thermal Spray Technology,* vol. 4 (2), pp. 185-194, 1995.

[6] „DLR - German Aerospace center," [Online]. Available: http://www.dlr.de. [Zugriff am July 2017].

[7] „Hydrogen from RES: pressurised alkaline electrolyser with high efficiency and wide operation range," [Online]. Available: http://www.reselyser.eu/. [Zugriff am April 2017].

[8] I. Ulleberg, „Modeling of advanced alkaline electrolyzers: a system simulation approach," *International Journal of Hydrogen Energy,* Bd. 28, pp. 21-23, 2003.

[9] O´Hayre, Ryan; Cha, Suk-Won; Colella, Whitney and Pinz, Fritz B., Fuel Cell Fundamentals, Colorado: Wiley, 2009.

[10] Zeng, Kai and Zhang, Dongke, „Recent progress in alkaline water electrolysis for hydrogen production and applications," *Progress in Energy and Combustion Science,* Bd. 36, pp. 307-326, 2010.

[11] Wittmaier, Dennis, et al., „Bifunctional, Carbon-Free Nickel/Cobalt-Oxide Cathodes for Lithium-Air Batteries with Aqueous Alkaline Electrolyte," *Electrochimica Acta,* Bd. 149, pp. 355-363, 2014.

[12] K. Schultze und H. Bartelt, „Formation and reduction of nickel(II)hidroxide on raney-nickel electrodes and its influence on the hydrogen overvoltge," *International Journal of Hydrogen Energy,* Bd. 17, pp. 711-718, 1992.

[13] Bing, Liu et al., „Cyclic voltammetric studies of stabilized a-nickel hydroxide electrode," *Journal of Power Sources,* Bd. 79, pp. 277-280, 1999.

[14] D. S. Hall, C. Bock und B. R. MacDougall, „The Electrochemistry of Metallic Nickel: Oxides, Hydroxides, Hydrides and Alkaline Hydrogen Evolution," *Journal of Electrochemical Society,* Bd. 160, pp. 235-243, 2013.

[15] A. Nelson, Phillip et al., „Mesoporous Nickel/Nickel Oxide - a Nanoarchitectured Electrode," *American Chemical Society,* Bd. 14, pp. 524-529, 2014.

[16] Dong, H. X. et al., „Oxidation behaviour of porous NiAl prepared through reactive synthesis," *Materials Chemistry and Physics,* Bd. 122, pp. 417-423, 2010.

[17] J. W. D. Callister, Materials science and engineering: an introduction - 7th edition, United States of America: John Wiley & Sons, Inc., 2007.

[18] V. K. Sikka, „Intermetallic-based high-temperature materials," Oak Ridge National Laboratory, Oak Ridge, Tenesse, 2008.

[19] Reutzel, S. et al., „Non-equilibrium solidification of intermetallic compounds in the Ni-Al alloy system," in *TMS Annual Meeting*, Orlando USA, 2007.

[20] López, G.A., et al. , „Kinetic behaviour of diffusion-soldered Ni/Al/Ni interconnections," *Materials Chemistry and Physics,* Bd. 78, pp. 459-463, 2002.

[21] Sanches, Luciana S. et al., „Characterisation of electrochemically deposited Ni-Mo alloy coatings," *Electrochemical Communications,* Bd. 6, pp. 543-548, 2004.

[22] Wu, Liang et al.;, „The stability of hydrogen evolution activity and corrosion behavior of porous NiAlMo electrode in alkaline solution during long-term electrolysis," *Energy,* Bd. 67, pp. 19-26, 2014.

[23] Fabbri, E. et al., „Developments and perspectives of oxide-based catalysts for the oxygen evolution reaction," *Catalysis Science & Technology,* Bd. 4, pp. 3800-3821, 2014.

[24] Ichikawa, H. et al., „Durability and Activity of Modified Nickel Anode for Alkaline Water Electrolysis," *EDS Transactions,* Bd. 58 (33), pp. 9-15, 2014.

[25] Singh, R.-N. et al., „Thin films of C0304 and NiCo204 obtained by the method of chemical spray pyrolysis for electrocatalysis III. The electrocatalysis of oxygen evolution," *Journal of Applied Electrochemistry,* Bd. 20, pp. 442-446, 1989.

[26] Y.-C. Liu und J. A. a. S. J. A. Koza, „Conversion of electrodeposited Co(OH)2 to CoOOH and Co3O4, and comparison of their catalytic activity for the oxygen evolution reaction," *Electrochimica Acta,* Bd. 140, pp. 359-365, 2014.

[27] Wittmeir, Dennis, et al., „Higly stable carbon-freeAg/Co3O4 cathode for Li-air batteries: Electrochemical and structural investigations," *Advances Energy Materials,* 2015.

[28] Krishnan, K. Hari et al., „An Overall Aspect of Electroless Ni-P Depositions—A Review Article," *Metallurgical and Materials Transactions,* Bd. 37A, pp. 1917-1926, 2006.

[29] „Oerlikon Metco," [Online]. Available: https://www.oerlikon.com. [Zugriff am May 2017].

[30] S. C. F. Araujo, „Electrochemical study of under-potential deposition processes on transition metal surfaces," University of Texas, Texas, 2006.

[31] Wang, Li, et al., „Improving the activity and stability of Ir catalysts for PEM electrolyser anodes by SnO2:Sb aerogel supports: does V addition play an active role in electrocatalysts?," *Journal of Materials Chemistry A,* Bd. 5, pp. 3172-3178, 2017.

[32] Knies, Sonja, et al., „Structure formation of activated nickel catalyst during caustic leaching of a nickel-aluminium alloy," 2001.

[33] D. S. Hall, C. Bock und B. R. MacDougall, „The electrochemistry of metallic nickel: oxides, hydroxides, hydrides and alkaline hydrogen evolution," *Journal of Electrochemical Society,* Bd. 160 (3), pp. F235-F243, 2013.

[34] „Wikipedia, the free encyclopedia," [Online]. Available: https://en.wikipedia.org/wiki/Silver_oxide. [Zugriff am July 2017].

[35] Zamora-Garcia, I. R., et al., „Thermodynamic and electrochemical study on the mechanism of formation of Ag(OH)4−in alkaline media," *Electrochimica Acta,* Bd. 111, pp. 268-274, 2013.

[36] „Geochemical Instrumentation and Analysis," [Online]. Available: http://serc.carleton.edu/research_education/geochemsheets/techniques/SEM.html. [Zugriff am May 2017].

[37] „MEE - Materials Evaluation and Engineering, Inc.," [Online]. Available: http://www.mee-inc.com/hamm/energy-dispersive-x-ray-spectroscopyeds/. [Zugriff am May 2017].

[38] „Wikipedia, the free encyclopedia," [Online]. Available: https://upload.wikimedia.org/wikipedia/commons/thumb/4/49/Electron_Interaction_with_Matter

.svg/1061px-Electron_Interaction_with_Matter.svg.png.

[39] „EAG Laboratories," [Online]. Available: http://www.eag.com/x-ray-diffraction-xrd/. [Zugriff am May 2017].

[40] „Particle Analytical - Analysis for the Pharmaceutical Industry," [Online]. Available: http://particle.dk/methods-analytical-laboratory/xrd-analysis/. [Zugriff am May 2017].

[41] Rayes, Youssef El et al., „Analytical methods for wine polyphenols analysis and for their antioxidant activity evaluation.," in *Phenolic Composition, Classification and Health Benefits*, Nova Publishers, 2014, pp. 71-102.

[42] „Chemistry Libretexts," [Online]. Available: https://chem.libretexts.org/Core/Analytical_Chemistry/Instrumental_Analysis/Cyclic_Voltammetry. [Zugriff am May 2017].

[43] „Department of Chemical Engineering and Biotechnology of University of Cambridge - Linear Sweep and Cyclic Voltametry: The Principles," [Online]. Available: http://www.ceb.cam.ac.uk/research/groups/rg-eme/teaching-notes/linear-sweep-and-cyclic-voltametry-the-principles. [Zugriff am June 2017].

[44] Won, Yu-Ra and Kim, Dong-Su, „The influence of temperature on the recovery reaction of silver based on the pourbaix diagram," *Journal of Korean Institute of Resources Recycling,* Bd. 21, pp. 74-81, 2012.

[45] Sato, N. and and Shimizu, Y., „Anodic oxide on silver in alkaline solution," *Electrochimica Acta,* Bd. 18, pp. 567-570, 1973.

[46] Chade, Daniel, et al., „Evaluation of Raney nickel electrodes prepared by atmospheric plasma spraying for alkaline water electrolysers," *International Journal of Hydrogen Energy,* Bd. 38, pp. 14380-14390, 2013.

[47] Sanches, Luciana S., et al., „Electrodeposition of Ni–Mo and Fe-Mo Alloys from Sulfate-Citrate Acid Solutions," *Sociedade Brasileira de Química,* Bd. 14, pp. 556-563, 2003.

[48] Lezna, R.O.; de Tacconi, N. R. and Arvia, A. J. , „The electrochemical behaviour of iridium/silver loaded iridium electrodes in acid electrolytes," *Journal of Electrochemical Chemistry,* Bd. 185, pp. 109-117, 1984.

[49] Knies, S., „Herstellungsprozess und Mikrostruktur von aktivierten Nickelkatalysatoren," Technische Universität Darmstadt, 2001.

Appendix A

The double layer effect is created by accumulated ions that form two mobile layers of solvent molecules and adsorbed species on the surface of the electrode. The one in the electrode side is relatively more ordered than the one in contact with the electrolyte. This layer creates an interfacial potential difference between the electrode surface and the electrolyte leading to a capacitive behaviour of the electrode reactions. Figure 29, is an illustration of the double layer effect existing in the surface of the electrode. This layer creates an interfacial potential difference between the electrode surface and the electrolyte leading to a capacitive behaviour of the electrode reactions.

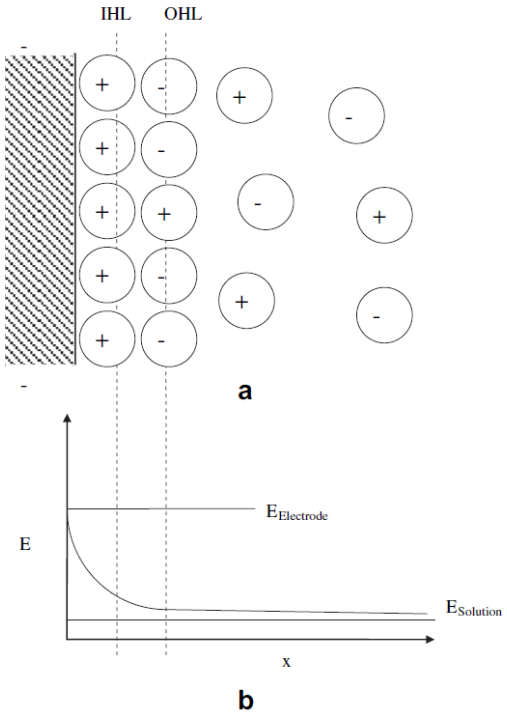

Figure 29 – Illustration of double layer and potential distribution near the electrode [10].

In water electrolysis, the cell overpotential reduce, although slightly, with increasing temperature, as seen in Figure 30 [10].

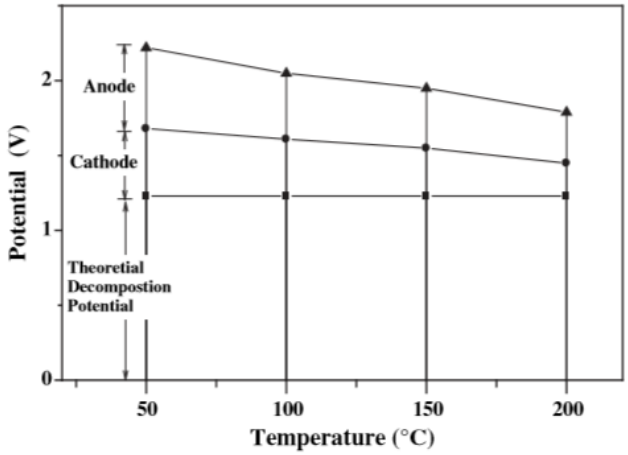

Figure 30 – Evolution of the cell overpotential with increase temperature [10].

Appendix B

SEM

Scanning electron microscopy is a characterization technique where a beam of electrons scans the sample surface originating a variety of signals that can be transformed into a picture. This picture reveals information about the external morphology, chemical composition, crystalline structure, and materials orientation on the surface of the sample [36].

EDX

Energy Dispersive X-Ray Spectroscopy is an analytical technique used to identify the chemical composition of a sample and is made along with SEM. The interaction of X-ray beams with each element results in a unique response (characteristic X-ray emission) that is detected, analysed, and afterwards recorded as a graph. Using the characteristic energy of each element's signal and its detected intensity the relative composition of the sample can be calculated. Figure 31 shows how the interaction between the rays and the surface takes place [37].

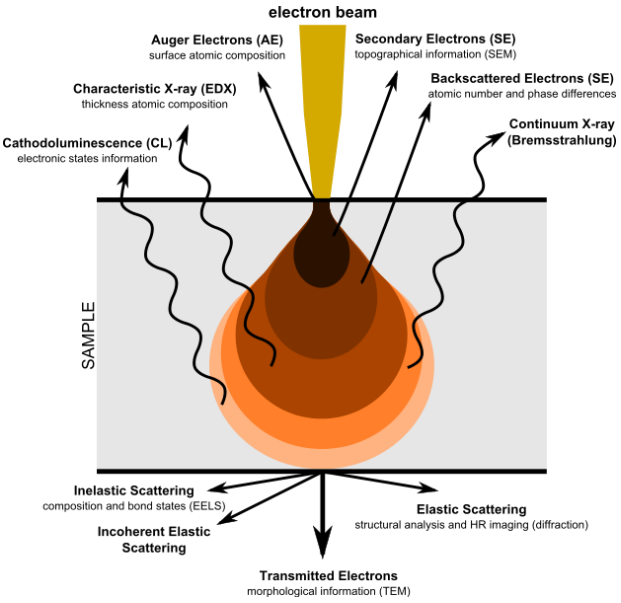

Figure 31 – Illustration of the interaction of the rays with the surface of the sample [38].

XRD

X-Ray Diffraction is a technique for characterizing crystalline materials providing information about the crystal structure, phase, preferred crystal orientation, average grain size, crystallinity, strain, crystal defects among other structural parameters. The X-rays are generated by a cathode ray tube, filtered to produce monochromatic radiation, concentrated in a set of parallel rays, and then

propelled onto the sample. The local distribution of these rays after interaction with the sample is then detected, processed, and registered as a graph that is unique for each material [39] [40].

Current-voltage measurements

Cyclic voltammetry

Cyclic voltammetry is a technique used to test the electrochemical behaviour of an electrode by cycling the potential and measuring the resulting current [12].

In this technique, the voltage is swept between two limits at a fixed rate for as many cycles as the user desires resulting in a graph as seen in the following picture. The first scan is called the forward scan and the opposite, the reverse scan. In case of the cyclic voltammogram seen in the Figure 32, the potential is scanned negatively from (a) to (d), forward scan, causing a reduction. This creates a cathodic current i_{pc} and a cathodic peak potential E_{pc} in (c). After the switching potential, (d), the potential scans positively from (d) to (g), reverse scan, causing the oxidation. This creates an anodic current, i_{pa} and an anodic peak potential E_{pa} in (f). The peaks appear when the entire compound is reduced or oxidized and the potential value of the peak allows recognizing which one it is.

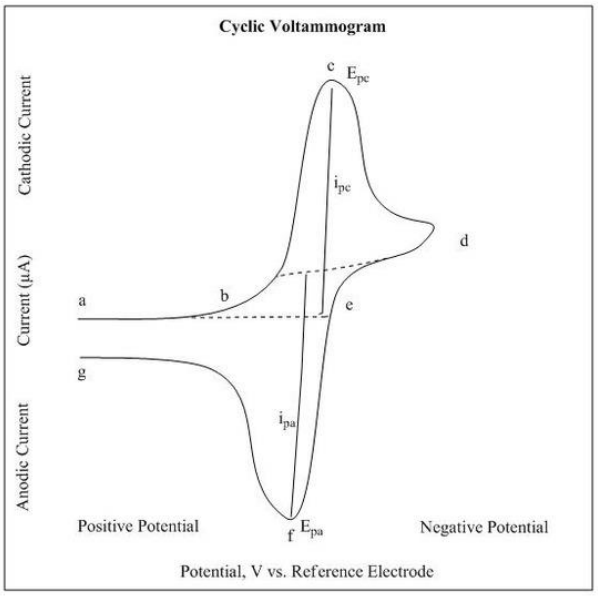

Figure 32 – Illustration of a typic cyclic voltammogram graph [41].

A cyclic voltammogram can give information about the electrochemical processes happening at the surface of the substrate under various conditions, as the presence of intermediates in the oxidation-reduction reaction and about the reversibility of the reaction. For example, a graph with the anodic and cathodic currents with the same size, as in the Figure 32, represents a fully reversible reaction and the intensity of the peaks is proportional to the extent of the reactions [42].

Some parameters must be chosen to make the CV analysis as the potential limits and the scan rate. In the potential limits must be included the potential of the reaction in study. In this work to different windows were chosen for cathodes and anodes. The lower potential limit for cathodes test was chosen taking into account the potential when the HER happens. In order to avoid the electrode destruction with oxidation or many reactions taking place in its surface, a low maximum voltage was chosen. For the anodes, the upper limit was chosen to include the start of OER and the lower limit was chosen, again, to exclude too many reactions taking place at the electrode surface. As seen before, the surface goes through several transformations that create strains and damages in the coating. For that reason, the window chosen for the study of the electrodes is small. When it comes to the slew rate, a balance between to effects must be achieved. The total current increases with increasing scan rate, which correspond to an increase of the charge the peaks, however, if the scan rate is too fast then the record quality decreases. The response of the electrode towards the scan rate change depends on the size of the diffusion layer and on the time taken to record the scan. In a slow voltage scan the diffusion layer will grow much further from the electrode in comparison to a fast scan. Consequently, the flux to the electrode surface is considerably smaller at slow scan rates than it is at faster rates. As the current is proportional to the flux towards the electrode the magnitude of the current will be lower at slow scan rates and higher at high rates. Therefore, a balance must be found and a scan rate of 5 $mV \cdot s^{-1}$ was found to be suitable for these tests [43].

Potentiostatic measurement

In a potentiostatic measurement the voltage is swept linearly or between two limits recording the current output and the ohmic resistance. The resulting graph is an i-V curve. From i-V curves it is possible to calculate approximately the activation energy, assuming that the ohmic loss is negligible towards the activation loss. If the current density is plotted in a log scale the curve presents a linear behaviour that can be described by the Tafel equation:

$$\eta = a + b \log i \tag{22}$$

The Tafel slope and the current density, *i*, are used to compare electrodes performances.

For both measurements, some important points must be considered. The steady state of the system must be achieved and the test conditions, as warm-up, temperature, slew rate, frequency and amplitude of the readings must be documented. To guarantee this, the cell must be operating for some time, usually 15 min before any test. To compare all samples the same conditions for their tests must be used [10].

Under-potential deposition (UPD)

A cyclic voltammogram of an Ag disk in 4.0 mol·L^{-1} NaOH is represented in Figure 33. The CV scan starts at lower values of potential which is increased in the forward scan and several silver oxides are formed (peaks A1, A2 and A3 in Figure 33). In the reverse scan, when the potential decreases, silver oxides are reduced back to metallic Ag and, because of the UPD effect explained above, is expected that a monolayer of metallic Ag be deposited in the Ni surface potentials higher than the standard Ag reduction value, which is 0.34 V vs RHE (Reversible Hydrogen Electrode) [35].

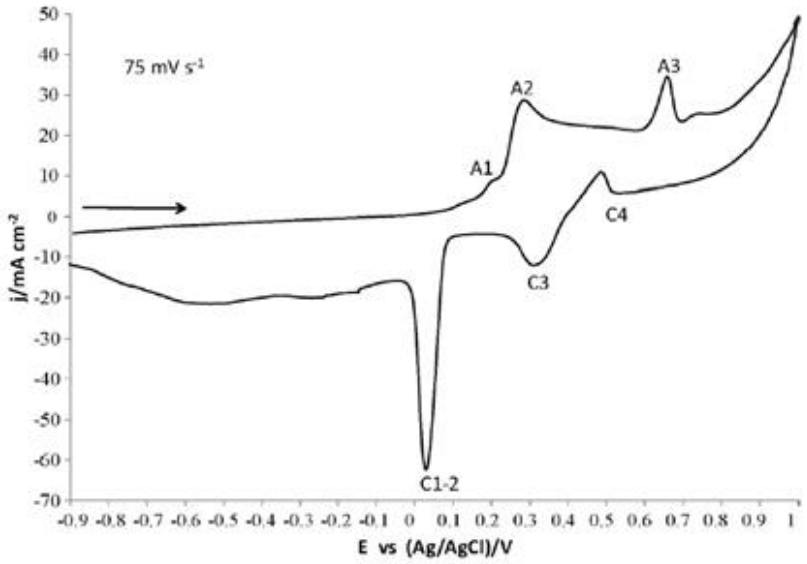

Figure 33 – Cyclic voltammogram of a Ag disk in 4.0 mol·L^{-1} NaOH [35].

The CV scan in Figure 33 was made in a potential window between -900 mV and 1000 mV vs Ag/AgCl with a slew rate of 75 mV·s^{-1}. Four peaks were obtained during the forward scan (direction of the arrow in Figure 33). For each anodic peak, in the forward scan, a cathodic peak exists, in the reverse scan. Because silver has several states of oxidation that depends on the voltage applied, several peaks can also be seen corresponding to different reactions taking place in the electrode and forming different silver oxides. Peak A1 is associated with the formation of a AgOH–$Ag(OH)_2$–monolayer. The reaction creating the increase in current is:

$$Ag^+ + Ni + e^- \rightleftharpoons NiAg_{ads} \quad (23)$$

It is believed that the oxidation of silver happens in two steps, as in the following equations, each one corresponding to a different peak:

Peak A2: $2Ag + 2OH^- \rightleftharpoons Ag_2O + H_2O + 2e^-$ (24)

Peak A3: $Ag_2O + 2OH^- \rightleftharpoons 2AgO + H_2O + 2e^-$ (25)

The processes A1, A2 and A3 can be understood in the light of the Pourbaix diagrams in Figure 3. Upon inversion of the scan direction toward negative potentials, the reduction of Ag is made and three cathodic peaks appear. C4 most likely corresponds to the reduction of Ag_3O_4 to Ag_2O and C3 for the reduction of these species to Ag_2O. The peak labelled as C1–2 corresponds to the formation of metallic Ag, which is associated with the reduction processes of A1 and A2 [35].

To transform the given potentials versus Ag/AgCl reference electrode into voltage versus RHE reference electrode to compare with the tests made in the present work one must add +0.22 V to each potential vs Ag/AgCl.

The phase diagram of the system Ag-H_2O at 45 ^oC is represented in Figure 34 and the voltage was measured versus SHE reference electrode. The diagram shows that in alkaline solutions, Ag is easily oxidized to form Ag_2O at potentials higher than 0.5 V and concentrations of Ag higher than 10^{-4} mol·L^{-1} [35].

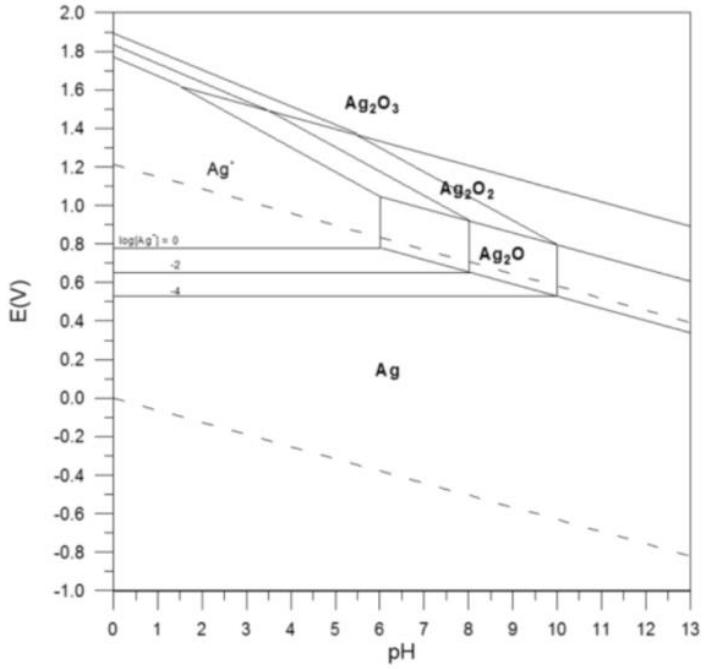

Figure 34 – Potential-pH phase diagram of Ag-H_2O system at 45 ^oC. The potential was measured vs SHE reference electrode [44].

Appendix C

The SEM images of the particles of NiAlMo (39/44/17 wt %) used in the coatings of the cathodes which were sprayed using APS are shown in Figure 35. The average particle size of the particles used was 20 µm. A comparison between these particles and the first coatings shows that some coatings contain entire particles that were not melted.

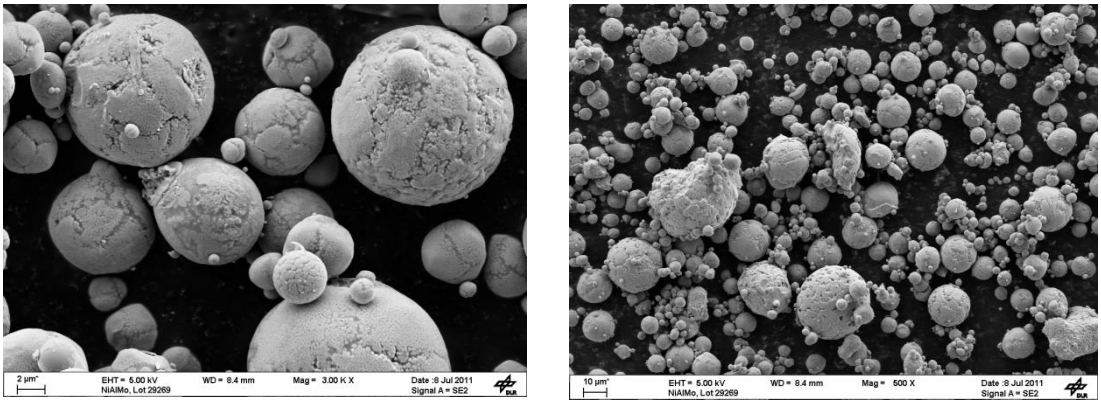

Figure 35 – SEM images of NiAlMo (39/44/17) powders used to spray the Ni steel punched metal sheet using APS. The electrodes coated with these powders were used as cathodes.

A linear scan of sample T17.001 is represented in Figure 36 showing how the composition changes with the distance from the surface. With the linear scan it is possible to associate the colours of the SEM image to the composition.

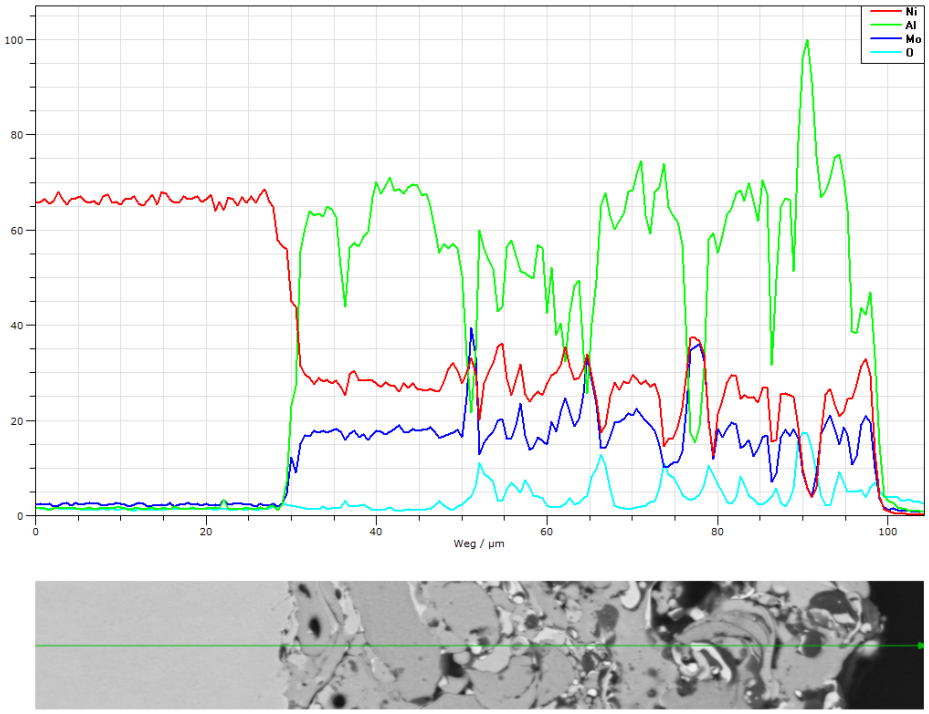

Figure 36 – Linear scan for as-sprayed sample T17.001, Ni substrate coated with NiAlMo.

After the coating process, the sample were leached and analysed with EDX. The resultant elemental maps for samples T17.001, T17.003 and T17.005 are showed in Figure 37. The samples chosen to analyse were the ones sprayed with lowest (T17.001) and highest (T17.005) speed plasma jet and the sample sprayed with the medium speed plasma jet (T17.003).

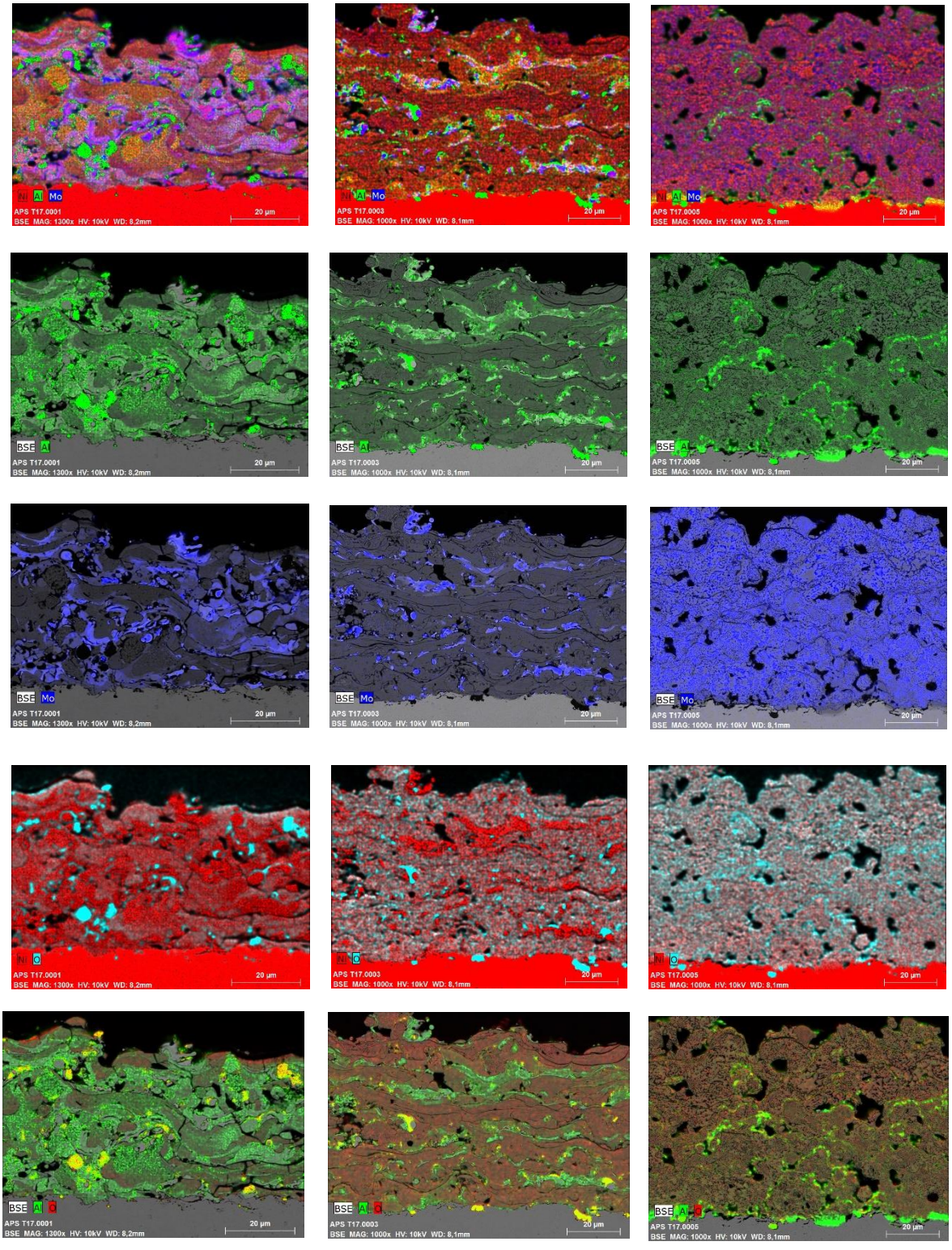

Figure 37 – EDX images of elemental distribution of the leached coatings of NiAlMo coated with different plasma jet velocities under a Ni substrate. The EDX images belong to samples T17.001 (lowest plasma speed), T17.003 and T17.005 (highest plasma speed).

Appendix D

In order to see the evolution of the performance of the electrodes, the cyclic voltammograms at different days of all the cathodes are represented in Figure 38. As explained in section 3.5.1, three cyclic voltammograms were performed at 70 ^{o}C in a 30% KOH bath, with a slew rate of 5 mV.s^{-1}. The CVs show at what potential the OER occurs and if other chemical activity is occurring during the tests. In Figure 38 is only represented the third cycle for each cathode because there is no difference between first, second and third cycle so it is possible to assume that it is stable with no further changes occurring on the surface and therefore the third cycle was taken. The cyclic voltammograms were made with the corrected voltage calculated by Equation 16 using the measured impedance values in Table 7.

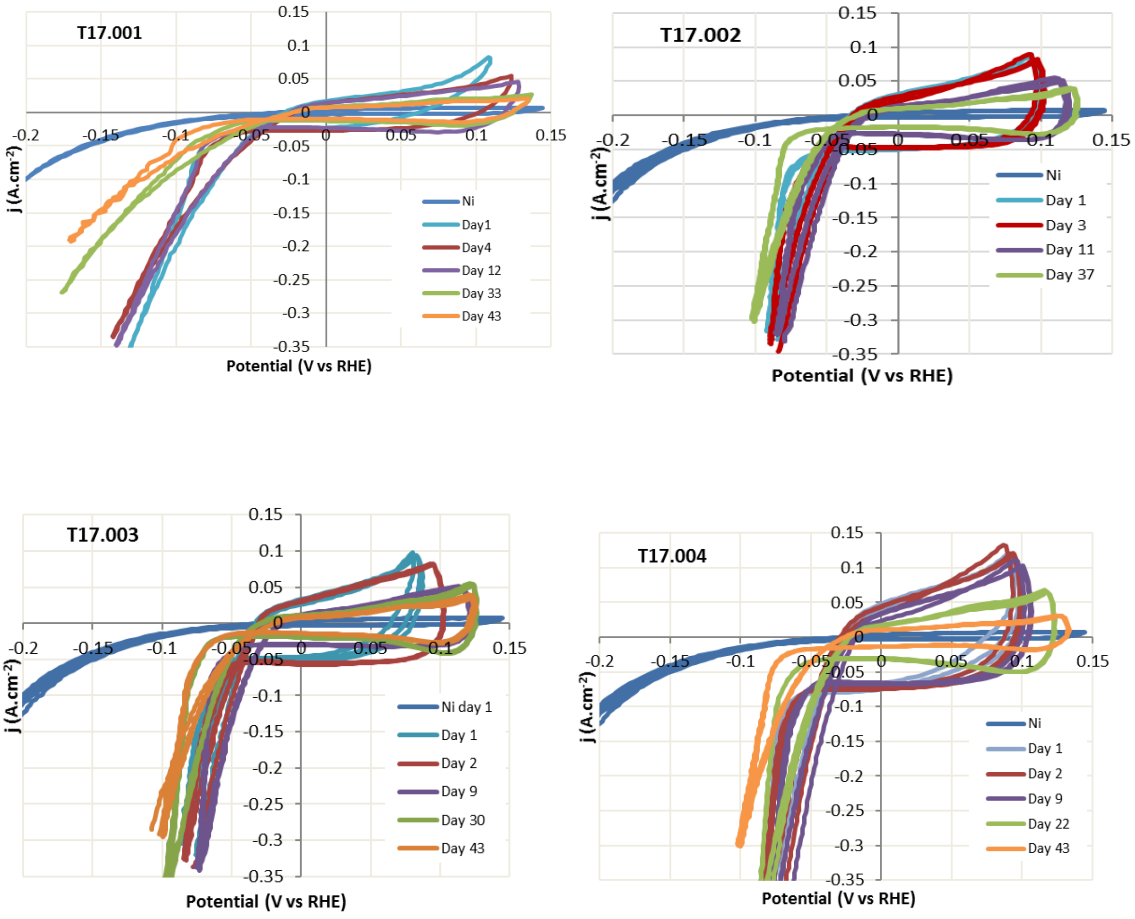

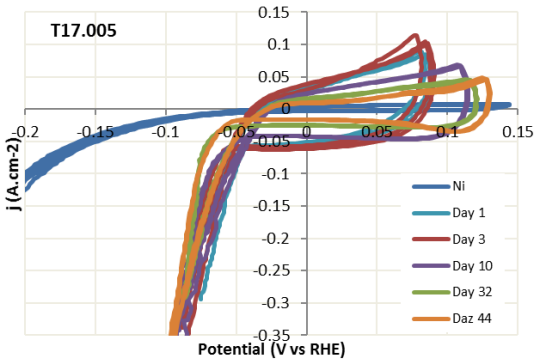

Figure 38 –Cyclic voltammograms for Ni coated with Raney-nickel NiAlMo samples T17.001 to T17.005 versus uncoated Ni electrode, in 30 % KOH solution at 5 mV·s^{-1} and 70 ^{o}C for the 3rd cycle at different times.

An illustration explaining the processes that take place during the cyclic voltammetry is represented in Figure 39. The CV used as example was the first day CV of sample T17.004.

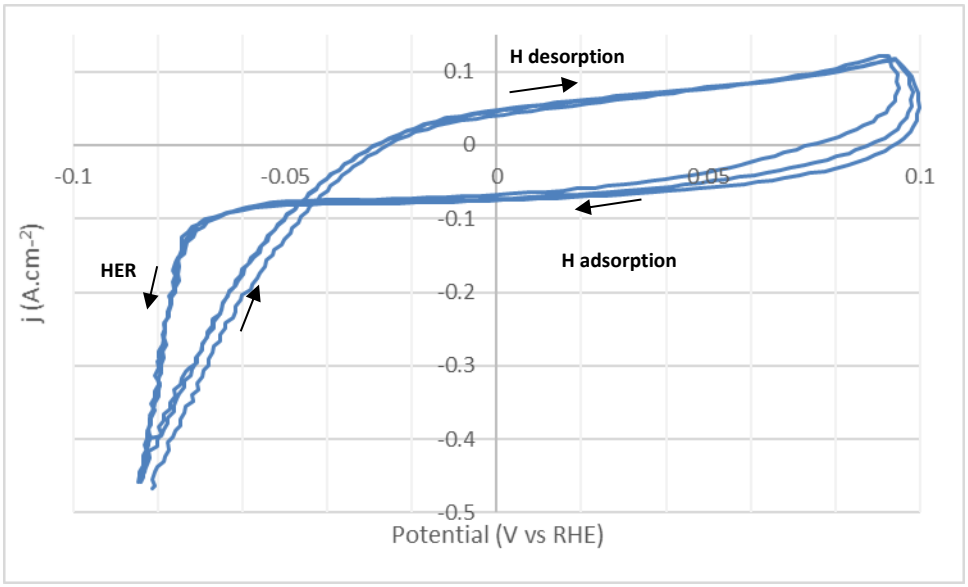

Figure 39 – Illustration clarifying the processes taking place during the CV. The arrows indicate the direction of the scan. The image shows the IR-corrected cyclic voltammograms for Ni electrode coated with Raney-nickel NiAlMo, sample T17.004 in 30 % KOH solution at 5 m·s^{-1} and 70 ^{o}C for the 3rd cycle. The correction was made with the impedance values in Table 7.

Appendix E

The SEM images of the NiAl particles sprayed by APS in the anodes coating are shown in Figure 40. Their shape and size can be compared with the particles in the coatings in chapter 4.2.1 and it is possible to identify that some particles were not properly melted.

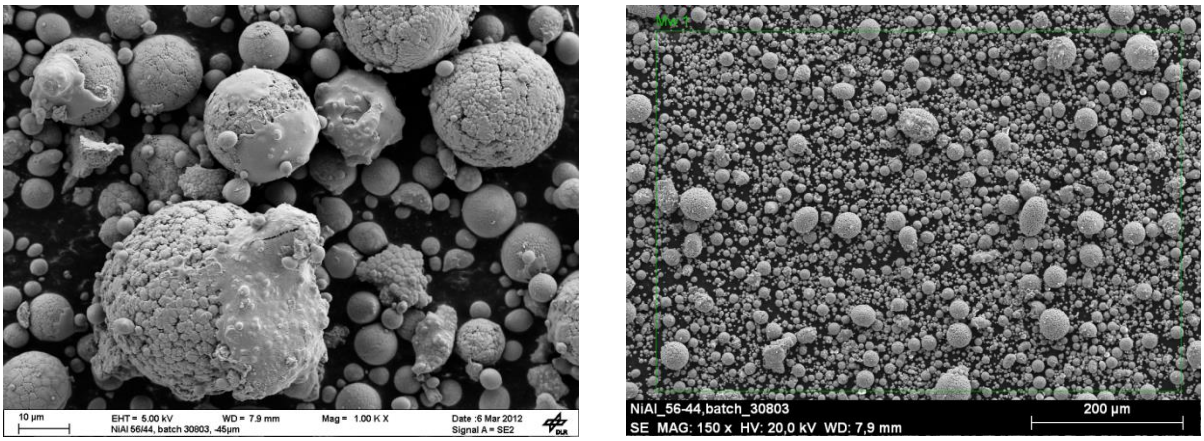

Figure 40 - SEM images of NiAl (56/44 wt %) powders used to spray the Ni expanded metal sheet using APS. The electrodes coated with these powders were used as anodes.

The XRD measurement of the NiAL powder is represented in Figure 41, where it is possible to see that both Ni_2Al_3 and Ni_3Al structures were present. Ni_3Al, which is present in bigger amount, is the responsible for the surface area increase after leaching.

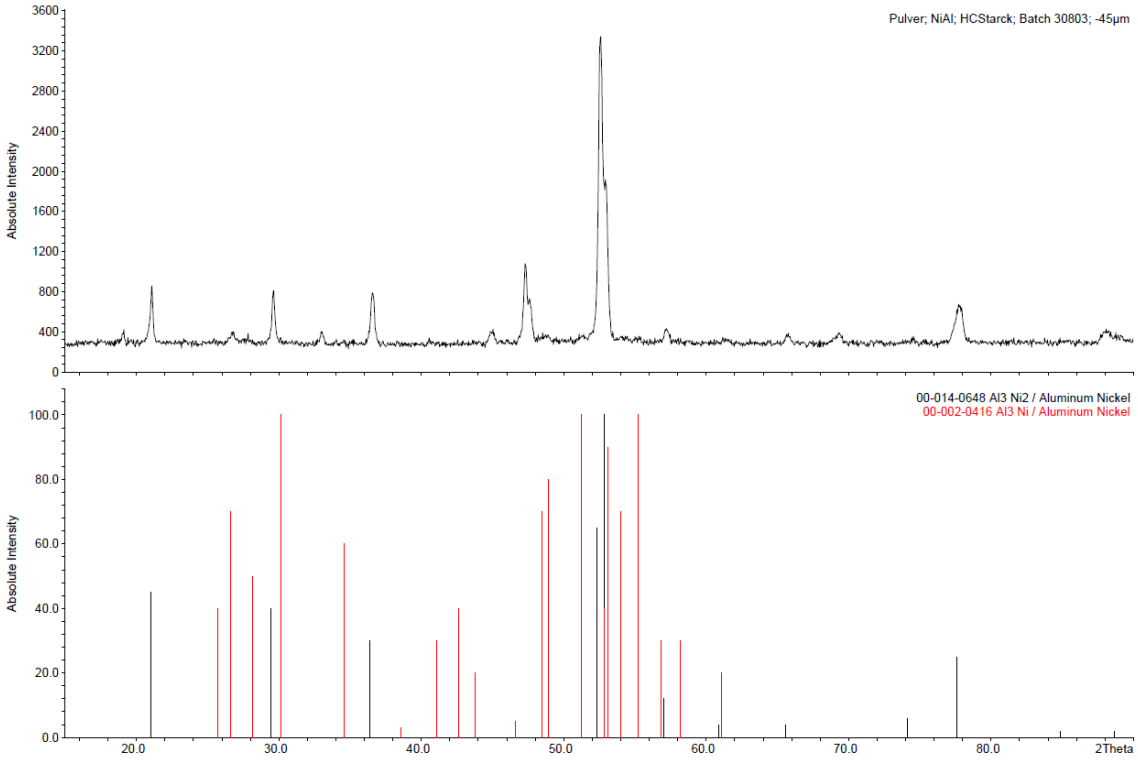

Figure 41 – XRD measurement of the NiAl powder used for the anodes (Batch: 30803).

Table 11 shows the normalized values by Ni amount in order to compare the quantity of each element with Ni. For the anodes, the amount of Ni was not the same for all electrodes, so the normalized values allow to have a better understanding of the leaching efficiency.

Table 11 – Normalized values of the EDX measurements results by Ni content in wt %.

wt %	O/Ni	Al/Ni	P/Ni	Co/Ni	Ag/Ni
T17.025.6 NiAl	20.81	20.97	-	-	-
T17.025.5 NiAl +P	26.20	17.04	0.46	-	-
T17.027 NiAl + Co_3O_4	24.81	51.27	-	59.76	-
T17.028 NiAl + Co_3O_4 + Ag	60.36	68.35	-	100.00	119.03

Figure 42 shows a line scan analysis of the electrode that went through the heat and P treatment to see how P is distributed inside the coating. It can be seen that in the surface there is more P than deeper in the coating.

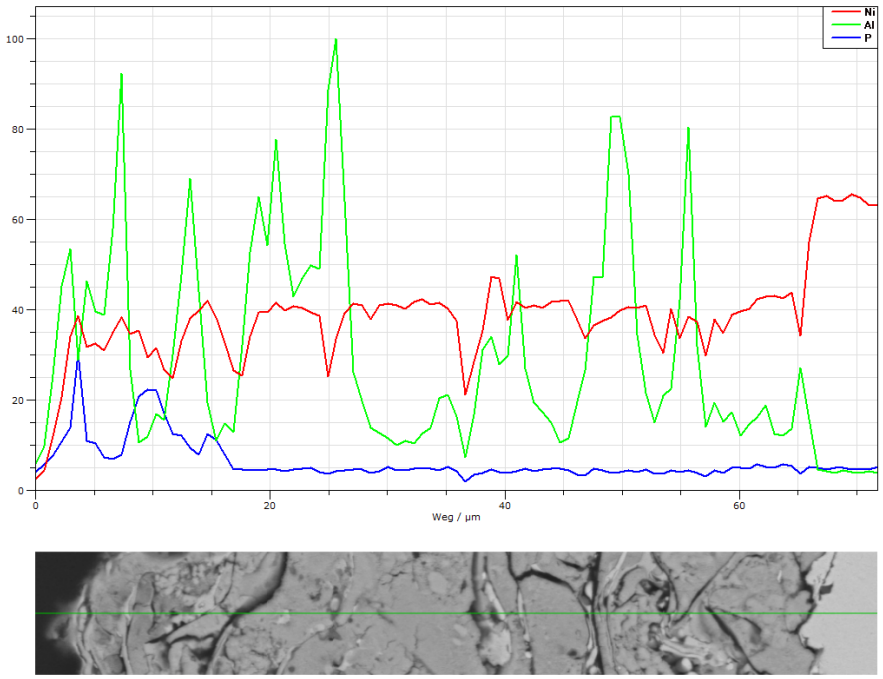

Figure 42 - EDX for as-sprayed sample T17.025.5 (top), SEM image with line used for the line scan in same scale (bottom).

The EDX images of the leached Ag/Co_3O_4/NiAl coating are represented in Figure 43. The leaching process was made in a 30 % KOH bath, at 80 ^{o}C for around 24 h.

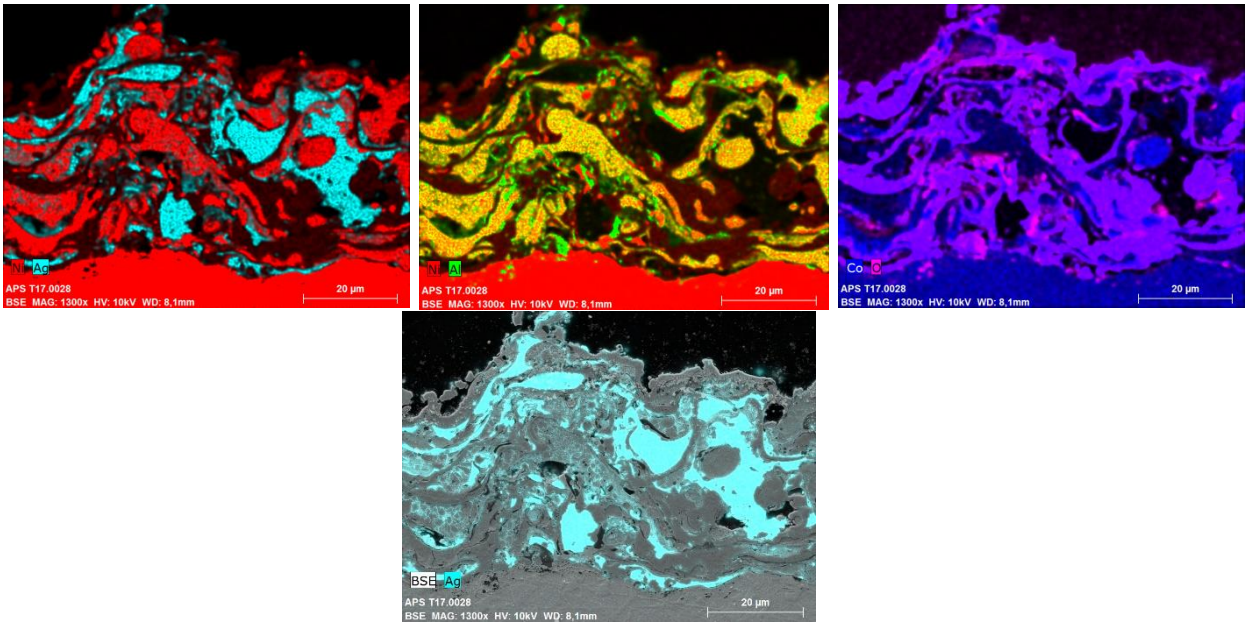

Figure 43 – EDX images of elemental distribution of leached Ag/ Co_3O_4/NiAl coating sprayed using APS above a Ni strechmetal electrode; sample T17.027.

Appendix F

An illustration explaining the direction of the scan during the cyclic voltammetry is represented in Figure 44. The CV used as example was the first day CV of sample T17.025.6. During the forward scan, an oxidation takes place, where the oxidation of Ni^{3+} to Ni^{2+} takes place.

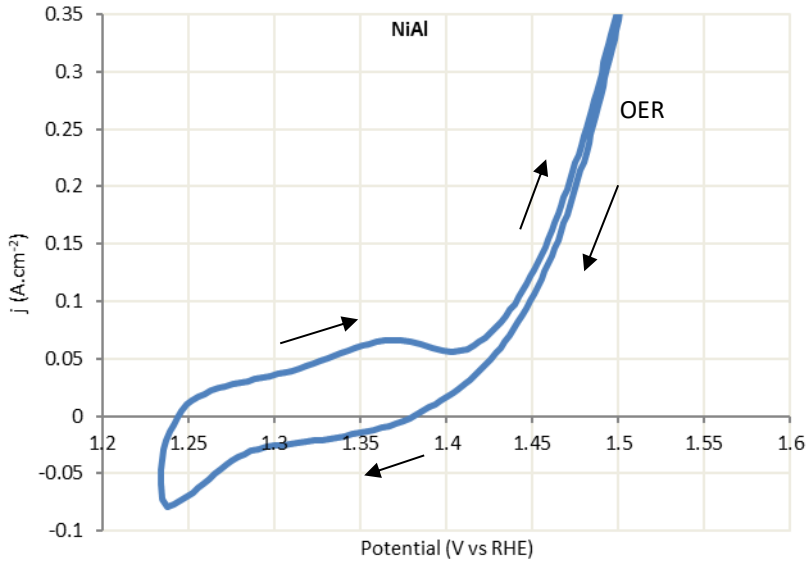

Figure 44 – Illustration clarifying the processes taking place during the CV. The arrows indicate the direction of the scan. The image shows the IR-corrected cyclic voltammograms for Ni electrode coated with Raney-nickel NiAl, sample T17.025.6 in 30 % KOH solution at 5 $mV \cdot s^{-1}$ and 70 ^{o}C for the 3rd cycle. The correction was made with the impedance values in Table 12.

The measured values of impedance used to calculate the IR-corrected values are summarized in Table 12 for each day and each sample.

Table 12 - Measured impedance resistance in the test bench used to calculate the I-V corrected values for all the coated Ni anodes.

Impedance	**1st day**	**2nd day**	**9th day**	**19th day**	**24th day**	**30th day**	
T17.025.6 NiAl	111	107	111	114	-	-	-
T17.025.5 NiAl + P	180	164	169	162	166	168	-
Impedance	**1st day**	**2nd day**	**9th day**	**13th day**	**16th day**	**20th day**	**21st day**
T17.027 NiAl + Co_3O_4	107	107	109	140	111	130	117
T17.028 NiAl + Co_3O_4 + Ag	159	154	151	-	-	-	-